Published October 31, 2019

Original Research

Core Ideas

- In the proposed model, the wilting point and porosity are a function of organic matter.
- In organic-rich soil, the model improves accuracy of the microwave radiative transfer model.
- The model is applicable for both portable and satellite soil moisture sensors.

A Dielectric Mixing Model Accounting for Soil Organic Matter

Chang-Hwan Park,* Carsten Montzka, Thomas Jagdhuber, François Jonard, Gabrielle De Lannoy, Jinkyu Hong, Thomas J. Jackson, and Volker Wulfmeyer

Most dielectric mixing models have been developed for mineral soils without extensive consideration of organic matter (OM). In addition, when used for in situ measurement, most of these models focus only on the real part of the effective dielectric constant without the corresponding imaginary part. Organic matter fractions in soils are found globally (57%), with an especially significant amount in the boreal region (17%). Without proper consideration of OM in dielectric mixing models and subsequent microwave radiative transfer modeling, brightness temperature (TB) calculations may be erroneous. This would lead to uncertainties in the estimation of higher level products, such as soil moisture retrievals from portable soil moisture sensors (e.g., time-domain reflectometers) or passive microwave sensors onboard the Soil Moisture Active Passive (SMAP), Soil Moisture and Ocean Salinity (SMOS), and Advanced Microwave Scanning Radiometer (AMSR2) satellites. We incorporated OM into a dielectric mixing model by adjusting the wilting point and porosity according to the OM content, i.e., the effective soil dielectric constant decreases with higher OM due to a decrease in the fraction of free water and an increase in bound water. With the proposed soil parameters in the dielectric mixing model, high levels of OM increase the TB for a specific soil moisture by decreasing the microwave effective dielectric constant. The simulated TB better reproduced SMAP-observed TB (11% in RMSE) through the improvement of the effective dielectric constant (40% reduction in RMSE). We anticipate that the application of our approach can improve microwave-based surface soil moisture retrievals in areas with high OM.

Abbreviations: DMM, dielectric mixing model; ISMN, International Soil Moisture Network; NDVI, normalized difference vegetation index; OM, organic matter; RTM, radiative transfer model; SM, soil moisture; SMAP, Soil Moisture Active Passive; SMOS, Soil Moisture and Ocean Salinity; TB, brightness temperature; TDR, time-domain reflectometry; ubRMSE, unbiased root mean square error; VOD, vegetation optical depth.

C.-H. Park, National Institute of Meteorological Sciences, Earth System Research Division, Korea Meteorological Administration (KMA), Jeju, Republic of Korea; C. Montzka and F. Jonard, Forschungszentrum Jülich GmbH, Institute of Bio- and Geosciences: Agrosphere (IBG-3), 52428 Jülich, Germany; T. Jagdhuber, Microwaves and Radar Institute, German Aerospace Center (DLR), 82234 Weßling, Germany; F. Jonard, Earth and Life Institute, UCLouvain, 1348 Louvain-la-Neuve, Belgium; G. De Lannoy, Dep. of Earth and Environmental Sciences, KU Leuven, B-3001 Heverlee, Belgium; J. Hong, Ecosystem-Atmosphere Process Lab., Dep. of Atmospheric Science, Yonsei Univ., Seoul, 03722 Republic of Korea; T.J. Jackson, Hydrology and Remote Sensing Lab., USDA, Beltsville Agricultural Research Center, Beltsville, MD 20705; V. Wulfmeyer, Institute of Physics and Meteorology, Univ. of Hohenheim, 70599 Stuttgart, Germany. *Corresponding author (chpark2@kma.go.kr; ecomm77@gmail.com).

Received 14 Apr. 2019.
Accepted 17 Sept. 2019.

Citation: Park, C.-H., C. Montzka, T. Jagdhuber, F. Jonard, G. De Lannoy, J. Hong, T.J. Jackson, and V. Wulfmeyer. 2019. A dielectric mixing model accounting for soil organic matter. Vadose Zone J. 18:190036. doi:10.2136/vzj2019.04.0036

Passive microwave satellite missions such as the Soil Moisture Active Passive (SMAP) (Entekhabi et al., 2010) and Soil Moisture and Ocean Salinity (SMOS) (Kerr et al., 2010) missions currently provide information about global soil moisture. In the process of such soil moisture estimation from microwave radiation observations, several factors may introduce uncertainty. For example, the misspecification of the vegetation, soil surface roughness, or physical properties of the soil in a radiative transfer model (RTM) can lead to erroneous soil moisture estimates (Babaeian et al., 2019). In the RTM, dielectric mixing models (DMMs) are particularly important in linking soil moisture to emissivity. The DMMs mix the dielectric properties of water and soil, while accounting for physical soil properties such as soil temperature and texture. Some DMMs has been widely used for remote sensing of soil moisture (Dobson et al., 1985; Mironov et al., 2009; Wang and Schmugge, 1980). A recent approach (Park et al., 2017) further considered standing water or saturated soil in the DMM. The efforts to build more sophisticated and accurate DMMs are important not only for soil moisture estimation from satellite data but also for ground-based soil moisture instruments such as time-domain reflectometry (TDR) (Robinson et al., 2003, 2005; Schaap et al., 2003; Wagner et al., 2013) and

ground-penetrating radar (Chan and Knight, 1999; Jonard et al., 2011; Klotzsche et al., 2018; Lambot et al., 2004a, 2004b, 2004c; Stoffregen et al., 2002) sensors.

Microwave electric fields induce dipole moments among water molecules, and this is the basis of the ability of microwave sensors to measure the interaction between electromagnetic waves and water molecules (dipoles) within a soil medium. The dielectric constant of free water is close to 80 at 1.4-GHz L-band microwave frequency owing to free rotational dipole motion when not in contact with the soil particles. The dielectric constant of liquid water decreases according to an increase in the microwave frequency or soil temperature in Debye relaxation. However, for water molecules bound to soil particles, the rotational moment is hampered by the force of attraction between the water molecules and the charged mineral particles. This reduces the dielectric constant to about one-third that of free water (Jones and Friedman, 2000). A valid estimation of soil moisture from microwave remote sensing measurements thus relies on our ability to accurately quantify the bound and free water fractions for the given soil sample. However, it is challenging to directly measure or estimate this phase information for soil water. One realistic solution is to approximate the ratio of bound and free water molecules in a DMM using the wilting point and porosity of the soil; bound water can occur when the soil moisture is lower than the wilting point, and free water is present when the soil moisture exceeds the soil porosity. Between these two points, there will be a mix of the two states. In this study, we improved a DMM by elaborating on the wilting point and the dry porosity terms for an organic-rich soil.

The organic matter (OM) of a soil may increase the specific surface area (O'Neill and Jackson, 1990), leading to an increase in the bound water fraction within the soil (Wigneron et al., 2017), and the pore-size distribution might shift from predominantly small pores to larger ones (Kellner and Lundin, 2001). In addition, OM, with its multipore structure, can reduce the space taken up by the dense minerals in the soil volume, as illustrated in Fig. 1.

Because of these microscopic and macroscopic mechanisms, an increase in OM may increase both the wilting point and porosity. This is supported by several pedotransfer functions, showing that the wilting point (Gupta and Larson, 1979; Jin et al., 2017; Rawls et al., 1982) and dry porosity (Saxton and Rawls, 2006; Tóth et al., 2015; Vereecken et al., 1989; Wösten et al., 1999) are higher for soils with higher OM content. If this impact of OM is incorporated into a DMM, the relationship between soil moisture and permittivity, and thus the relationship between soil moisture and brightness temperature (TB), will change accordingly. However, most currently used DMMs have been developed specifically for mineral soils only, and the specific impact of OM on soil permittivity in a DMM has not been widely studied. If information about the soil OM is not included, the forward modeling of the dielectric constant and, consequently, the TB is likely to be inaccurate, which in turn can lead to erroneous soil moisture estimates. This problem can be especially important for boreal regions, which cover about 13% of the world's land surface.

There are two solutions to this problem. Either the DMM structure can be addressed or the input parameters can be updated. Several empirical (Hallikainen et al., 1985; Roth et al., 1992; Topp et al., 1980) and semiempirical (Dobson et al., 1985; Mironov et al., 2009; Wang and Schmugge, 1980) DMMs are available for mineral soils, but only a few models have been developed with explicit consideration of OM. For soil moisture estimation using TDR sensors in organic-rich, sandy soil, various calibration models have been developed but are only applicable for the specific degree of OM (Bircher et al., 2016). Furthermore, a study (Mironov et al., 2015) also proposed a DMM for organic-rich soil that updates the bulk density in a previous version of the model (Mironov et al., 2009). This model has only been validated for thawed and frozen tundra in the 80 to 90% OM range. An empirical fitting model (Bircher et al., 2016) was proposed for organic-rich soil that can be applied to a specific soil texture and OM range. Though useful, these models were developed for a specific range of OM. They might be unreliable when applied to a wide range of OM for operational purposes. For more widespread applications, such as the generation of global soil moisture products, it is desirable to develop a model to cover the full range of OM contents. One

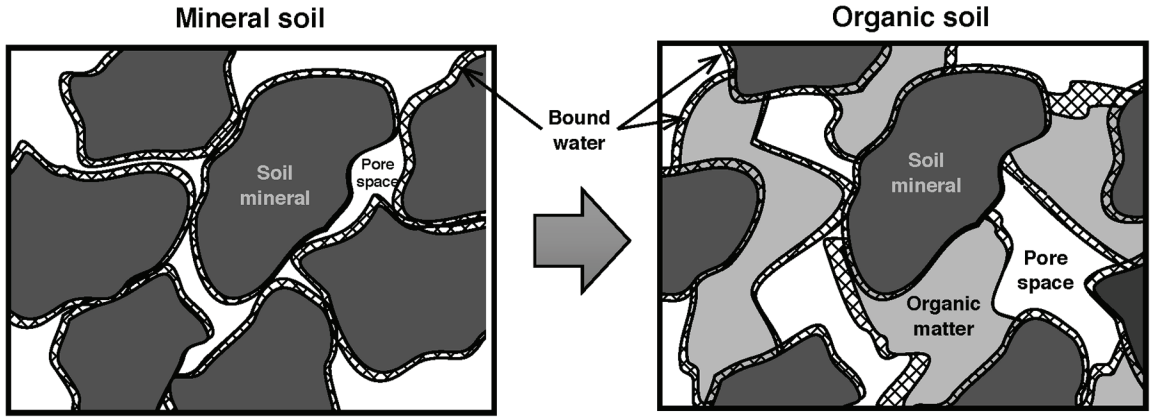

Fig. 1. Schematic illustration of the organic matter effect on the volume of pore (white space) and bound water (gridded layers) in macroscopic soil structure.

example of a global system that includes OM in the computation of global soil hydraulic parameters (De Lannoy et al., 2014) both for land surface and TB modeling is the Goddard Earth Observing System Land Data Assimilation System, used to assimilate SMOS TB (De Lannoy and Reichle, 2016a, 2016b) or SMAP TB (Reichle et al., 2017). However, the effect of OM (and the associated updated soil hydraulic parameters) on TB simulations has not been analyzed in detail.

In this study, we also propose a DMM that explicitly considers OM by computing updated soil hydraulic parameters and the effective dielectric constant of the soil for a wide range of different soil textures and OM concentrations. Our model builds further on the model of Park et al. (2017) by quantifying the wilting point and porosity based on the volumetric mixing ratio of the soil minerals and OM. The effect of OM on the soil dielectric constant and TB has yet to be fully investigated in the field of remote sensing (O'Neill and Jackson, 1990). We hypothesized that improvements in the representation of OM and soil texture in the model will result in more accurate simulations of the dielectric constant and TB so that we ultimately retrieve a more reliable soil moisture estimate from global spaceborne sensors.

We compared the widely used models (Bircher et al., 2016; Roth et al., 1992; Topp et al., 1980), which have been developed for use with portable soil moisture sensors, in the simulation of the real part of the effective dielectric constant. In addition, we also compared the most widely used DMMs for mineral soils developed by Wang and Schmugge (1980), Dobson et al. (1985), and Mironov et al. (2009), as well as a version of the model proposed by Mironov et al. (2015) modified to incorporate the OM in organic-rich soil.

Method

The main difference between the model presented in this study and existing mineral or OM calibration models is the inclusion of the wilting point and porosity for organic soils. The primary assumption in our approach is that accurate wilting point and porosity information is necessary in a microwave forward model because their changes due to the soil OM concentration affect the wave–surface interaction and subsequently the measured microwave TB. Figure 2 shows that the TB simulation model consists of three parts: (i) soil physics and hydraulic parameters, (ii) a DMM, and (iii) an RTM. We propose an improved forward model by introducing a new pedotransfer function for the wilting point and porosity (indicated by the black boxes in Fig. 2) to address uncertainty in soil moisture estimation (the blue box) based on ground-based observations and satellite-based remote sensing (the purple boxes).

Soil Physics

Figure 3 illustrates how the soil OM content affects (i) the wilting point and porosity calculated by the OM-related pedotransfer function models, (ii) the dielectric constant computed by the DMM proposed in this study, and (iii) the TB simulated by a RTM. We anticipated that by adjusting the wilting point and porosity as a function of OM (Fig. 3a), the soil hydraulic parameters will reduce the overestimation of the effective dielectric constant and the underestimation of the TB in organic-rich soils.

The previously reported physically based DMM (Park et al., 2017) contains both wilting point and porosity information, but these are determined by USDA soil texture classes. To improve on

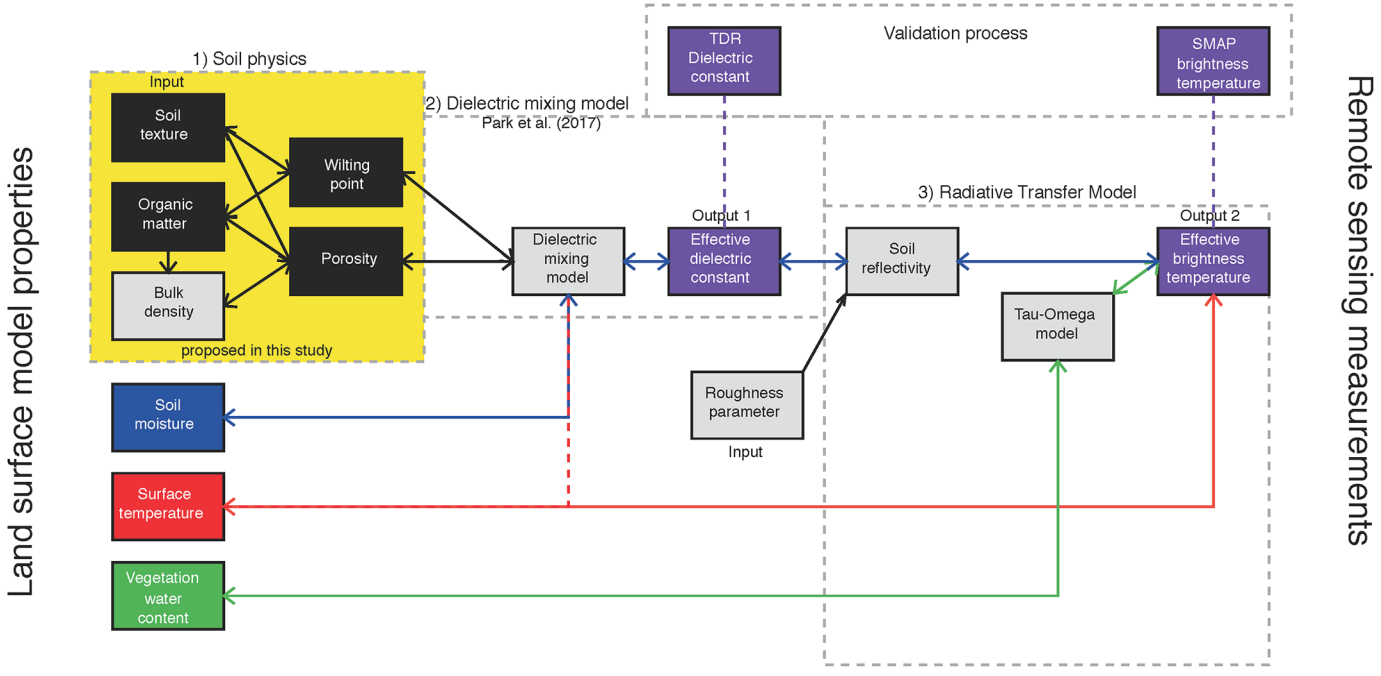

Fig. 2. Workflow of forward (left to right) model for calculation of the effective permittivity and brightness temperature of organic soils; soil moisture from International Soil Moisture Network measurements, surface temperature from Global Modeling and Assimilation Office GEOS-5 data, soil and vegetation opacity from MODIS-based product [MODIS 1000m MOD13A2(V005) normalized difference vegetation index [Chan et al., 2013]), and roughness parameter (Choudhury et al., 1979; Wang, 1983), which are currently applied as ancillary data for SMAP Level 3 products.

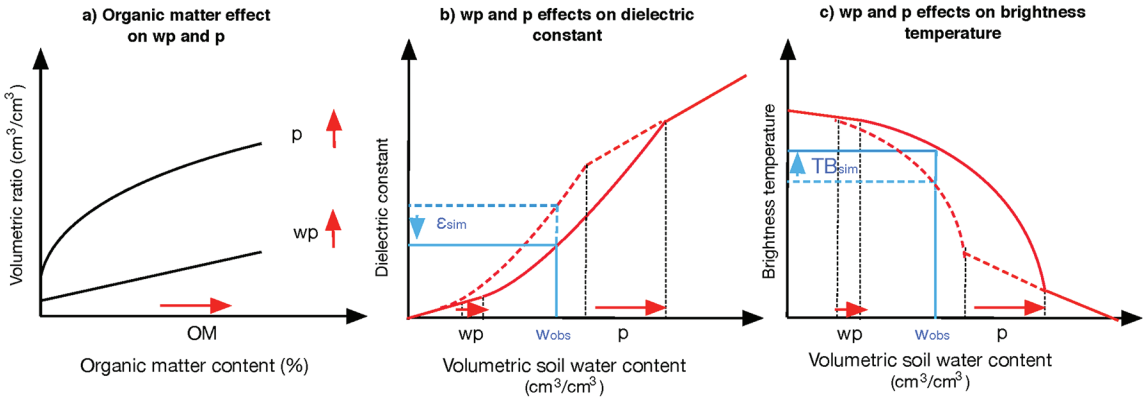

Fig. 3. Schematic illustration of organic matter effect on the wilting point (wp), porosity (p), the dielectric constant (ε), and brightness temperature (TB); dashed lines indicate curves for a mineral soil, while solid lines include organic matter.

this, the wilting point and porosity are calculated as a function of OM in the present study (the yellow box in Fig. 2). First, we apply a linear-type model for the wilting point (wp), similar to Jin's model (Jin et al., 2017):

$$\mathrm{wp} = 0.02982 + 0.089 v_{\mathrm{clay}} + 0.00786\,\mathrm{OM} \quad [1]$$

where v_{clay} is the volumetric mixing ratio of clay ($\mathrm{cm^3\ cm^{-3}}$), and OM is the organic matter content (%). Following this, for the calculation of soil porosity (p), the following pedotransfer function (Tóth et al., 2015) was applied in this study:

$$\begin{aligned} p = {} & 0.6819 - \frac{0.06480}{\mathrm{OC}+1} - 0.11900\,\mathrm{BD}^2 - 0.02668 \\ & + 0.1489 v_{\mathrm{clay}} + 0.08031 v_{\mathrm{silt}} + \frac{0.02321}{(\mathrm{OC}+1)\mathrm{BD}^2} \\ & + 0.01908\,\mathrm{BD}^2 - 0.11090 v_{\mathrm{clay}} - 0.2315 v_{\mathrm{silt}} v_{\mathrm{clay}} \\ & - 0.01197 v_{\mathrm{silt}} \mathrm{BD}^2 - 0.01068\, v_{\mathrm{clay}} \mathrm{BD}^2 \end{aligned} \quad [2]$$

where v_{silt} is the volumetric mixing ratio of soil silt ($\mathrm{cm^3\ cm^{-3}}$), BD is the soil bulk density ($\mathrm{g\ cm^{-3}}$), and OC is the soil organic C, defined as the OM divided by 1.72 (Stenberg et al., 2010) (%). Soil BD (Yang et al., 2014) is determined as

$$\mathrm{BD} = -0.039\,\mathrm{OM} + 1.2301 \quad [3]$$

The wilting point and porosity vary with soil aggregation associated with OM, but here we simply use the amount of OM in the calculation of these parameters such as in Eq. [1] and [2]. In addition, BD is not only determined by OM but also by the amount of vegetation components in the soil, such as roots and litter, and by individual agricultural practices. We will test whether the proposed model, outlined in Eq. [1–3], reasonably represents the effect of OM on the wilting point, porosity, and BD for high-OM regions despite these limitations.

Dielectric Mixing Models

Table 1 shows the dielectric mixing models tested in this study. All models listed in Table 1 simulate the real part of the effective dielectric constant, which can be compared with measurements from in situ sensors, such as TDR instruments. However, among all models, the Topp model (Topp et al., 1980) ($\mathrm{T_o}$ hereafter) and

Table.1. Description of the dielectric mixing models used in this study, with an indication of the variables used (O) or not used (X) for input. The organic matter content is used either as a constant (Δ) or as a variable within the bulk density by modification in this study (Δ*). The bottom part of the table ranks the models in terms of their performance for the evaluation of the dielectric constant vs. point samples and for the evaluation of brightness temperature (TB) simulations vs. SMAP observations.

Characteristic	Models for mineral soil†				Models for organic-rich soil‡				
	W	D§	M¶	P	$\mathrm{T_o}$	$\mathrm{R_o}$	$\mathrm{B_o}$	$\mathrm{M_o}$	$\mathrm{P_o}$
Real part	O	O	O	O	O	O	O	O	O
Imaginary part	O	O	O	O	X	X	O	O	O
Frequency	O	O	O	O	X	X	X	O	O
Temperature	O	O	O	O	X	X	X	O	O
Sand	O	O	O	O	X	X	X	O	O
Clay	O	O	O	O	X	X	X	O	O
Salinity	O	O	O	O	X	X	X	O	O
Wilting point	O	X	O	O	X	X	X	O	O
Porosity	O	O	X	O	X	X	X	X	O
Standing water	X	X	X	O	X	X	X	X	O
Damping effect	X	X	X	O	X	X	X	X	O
Organic matter	X	X	X	X	Δ	Δ	Δ	Δ*	O
	Evaluation results								
RMSE rank (ε)	5	7	8	4	3	6	2	9	1
Correlation rank (TB)	4	2	5	2	–	–	–	5	1
Bias rank (TB)	2	4	6	3	–	–	–	5	1
ubRMSE rank (TB)	5	2	5	3	–	–	–	3	1

† W, Wang and Schmugge (1980); D, Dobson et al. (1985); M, Mironov et al. (2009); P, Park et al. (2017).
‡ $\mathrm{T_o}$, Topp et al. (1980); $\mathrm{R_o}$, Roth et al. (1992); $\mathrm{B_o}$, (Bircher et al. (2016); $\mathrm{M_o}$, Mironov et al. (2015); $\mathrm{P_o}$, this study.
§ Operational model for SMOS and AMSR-E.
¶ Operational model for SMOS (since 2012) and SMAP.

Roth model (Roth et al., 1992) (R_o hereafter) DMMs cannot be used for a comparison with TB measurements because they cannot simulate the imaginary part of the dielectric constant. In addition, T_o, R_o, and the model of Bircher et al. (2016) (B_o hereafter) are only applicable to specific frequencies and soil textures because they do not account for OM variability despite their inclusion of organic soil.

The Dobson model (Dobson et al., 1985) (D hereafter) and Mironov model (Mironov et al., 2009) (M hereafter) were used operationally in SMOS, the Advanced Microwave Scanning Radiometer (AMSR-E), and SMAP Levels 2 and 3 soil moisture retrievals. These two models consider both the real and imaginary parts of the dielectric constant and reflect the variability in soil texture, temperature, and frequency. However, there are no OM-related variables, which may result in uncertainty in TB simulation for organic-rich soils. The Mironov model (Mironov et al., 2015) was based on a function of soil BD and considered OM effects implicitly by its statistical relationship with BD. Accordingly, it can be applied to organic-rich soils in tundra by applying a specific range of BD from 0.563 to 0.666 g cm^{-3} rather than a function of OM properties. To investigate its operational applicability for this range of OM content and the impact of OM variability, in this study the model of Mironov et al. (2015) has been extended by replacing the constant BD with the BD function in Eq. [3] (M_o hereafter).

The Park model (Park et al., 2017) (P hereafter) has recently been introduced for soil moisture estimation in mineral soils. The main difference between the P model and standard models such as M and D is the ability to simulate standing water (i.e., oversaturated soil conditions), which is critical for capturing soil states associated with surface runoff and flooding events. The P model also includes both wilting point and porosity information that can be linked to OM, as described in above. Our proposed model is based on the P model and considers organic matter explicitly (P_o hereafter). Therefore, the P_o model includes improvements on the P model and is suitable for organic-rich soil. The P_o model is further divided into P_or (an OM input from the SoilGrid1km database [Hengl et al., 2014] into the P model) and P_oh (OM input from the Harmonized World Soil Database [FAO, 2012] into the P model). Similarly to P_oh and P_or, M_o was also tested with these two different OM inputs (M_oh and M_or, respectively). Based on these modifications, we tested the effect of OM on the calculation of the effective dielectric constant and subsequent TB simulation via the RTM introduced below.

Radiative Transfer Model

The soil reflectivity of rough surfaces for horizontal (r_h) and vertical (r_v) polarization can be computed using Fresnel scattering coefficients multiplied by a roughness attenuation term (Escorihuela et al., 2007; Wang and Choudhury, 1981; Wigneron et al., 2001). The next step is the simulation of TB that considers canopy transmissivity and the static water fraction on the surface (see the Appendix for more information).

The forward simulation of the dielectric constant and TB (the purple boxes in Fig. 2) requires information about the soil mineral and OM content (the black boxes in Fig. 2), soil water (the blue box in Fig. 2), soil temperature (the red box in Fig. 2), and the vegetation component (the green box in Fig. 2). The forward simulation of the dielectric constant and TB can be evaluated by comparing them with TDR measurements of dielectric constants and SMAP TB measurements, respectively. Below, we evaluate the proposed forward model in terms of the dielectric constant and TB by comparing it, along with other published models (Table 1), against ground- and satellite-based measurements.

Validation of Simulated Dielectric Constant

Before comparing the various model simulations with SMAP TB, it is necessary to validate the simulation of the dielectric constant at the point scale because it can directly show the OM effect without attenuation by vegetation opacity and its heterogeneity effect due to scale difference in the comparison. The simulation of the dielectric constant is performed with the input of the soil moisture estimated from TDR and soil texture and OM information. The result of the simulation is compared with the real part of the dielectric constant measured by TDR and validated by the following statistics:

$$\text{Bias} = \frac{1}{n}\sum_{i=0}^{n-1}\left[\varepsilon_{\text{sim}}\left(\text{SM}_{\text{in-situ},i}\right) - \varepsilon_{\text{TDR},i}\right] \quad [4]$$

$$\text{RMSE} = \frac{1}{n}\sqrt{\sum_{i=0}^{n-1}\left[\varepsilon_{\text{sim}}\left(\text{SM}_{\text{in-situ},i}\right) - \varepsilon_{\text{TDR},i}\right]^2} \quad [5]$$

Validation of Simulated Brightness Temperature

A challenging task in the evaluation of point-based forward TB simulations is to deal with the innate spatial scale issue when these simulations are compared with satellite TB. More specifically, TB simulations are performed with the input of the point-scale in situ soil moisture (SM) and compared against SMAP TB on a 40-km grid scale. If the surface properties within a 40-km grid are homogeneous, the TB simulation using any point measurement from this area can represent 40-km-scale TB comparable to SMAP observations. On the contrary, if the surface is heterogeneous, the point-scale simulation can differ significantly from the SMAP TB. However, the temporal trend of the TB variability from any individual points within a SMAP grid should be synchronized with precipitation events and daily evaporation dynamics. Therefore, we evaluate the temporal bias of the approaches first and remove the bias for the calculation of the unbiased RMSE (ubRMSE), a score that is less affected by spatial heterogeneity:

$$\text{Bias}_t = \frac{1}{t}\sum_{i=0}^{t-1}\left[\text{TB}_{\text{sim}}\left(\text{SM}_{\text{in-situ},t}\right) - \text{TB}_{\text{SMAP},t}\right] \quad [6]$$

$$\text{ubRMSE} = \frac{1}{t}\sqrt{\sum_{i=0}^{t-1}\left\{\left[\text{TB}_{\text{sim}}\left(\text{SM}_{\text{in-situ},i}\right) - \text{Bias}_t\right] - \text{TB}_{\text{SMAP},i}\right\}^2} \quad [7]$$

After removing temporal bias, we can focus on the OM effect on the temporal variability of TB simulation. In addition, the correlation in temporal variability can also be the indicator for the improvement due to the OM consideration in the model under the minimal effect of the spatial heterogeneity. In this study, we applied the Pearson correlation in the evaluation. Finally, to investigate the OM effect on TB simulation across a larger domain, we forward calculate two-dimensional (2D) TB for the direct comparison with 2D SMAP TB across the test area. In this 2D experiment, the SMAP Level 3 SM rather than in situ SM is utilized as the soil moisture input to the RTM because a 2D soil moisture field is required in this simulation. For both the point and 2D simulations of TB, we rely on prior SM estimates that are retrieved using a TDR or satellite measurement. It is important to realize that both measurements probably suffer from a lack of accounting for OM.

Data

We investigate the impact of OM on the accuracy of dielectric constant and TB simulation by comparison with point-scale in situ measurements in mineral and organic-rich soils with a wide range of soil mineral mixing ratios. For this purpose, forward simulations have been performed with soil moisture content retrieved from TDR and validated with the measured real part of the dielectric constant collected from the data points in published studies (Bircher et al., 2016; Miyamoto et al., 2003; Roth et al., 1992; Wagner et al., 2013). Furthermore, in these studies the ancillary information such as the mixing ratio of sand, silt, and clay, soil salinity, soil temperature, and OM has been used as shown in Table 2. For simulation of the dielectric constant, soil salinity and temperature were assumed to be 0‰ and 20°C, respectively, based on previous studies (Bircher et al., 2016; Miyamoto et al., 2003; Roth et al., 1992). The number of sample data used in the validation is 431 (data points) and covers the OM content ranging from 0.31 to 69.00% and soil textures from sand to clay. This validation of the dielectric constant estimation focused only on the effect of OM in the dielectric constant simulation model by excluding the effects of vegetation attenuation.

To investigate the effect of OM in pixel simulations, pixel-based TB simulations were compared with spaceborne TB measurements. Soil information for the model inputs was obtained from the Harmonized World Soil Database (FAO, 2012) and the SoilGrids1km dataset (Hengl et al., 2014). In this comparison, we used SMAP retrievals (L3_SM_P V.2: horizontally polarized TB [radiometer], 36-km grid resolution, from descending [AM] mode [Chan et al., 201, 2018]) over tundra and boreal forest in Alaska, where OM content is typically very high (Bircher et al., 2012; Jones et al., 2007; Mironov et al., 2010, 2013, 2015; Rautiainen et al., 2012; Watanabe et al., 2012). In this study, the validation points listed in Table 3 were applied based on the availability of in situ measurements of complementary soil moisture and soil temperature over arctic and alpine tundra (Fig. 4), which were sampled from the Soil Climate Analysis Network (SCAN; National Water and Climate Center, 2018a) and Snow Telemetry (SNOTEL; National Water and Climate Center, 2018b) databases of the NRCS and distributed by the International Soil Moisture Network (ISMN) (Dorigo et al., 2013). For the comparison with measured TB, both the real and imaginary parts of the effective dielectric constant were required, and scatterplots were produced from 500 samples divided into four ranges according to OM contents. It should be noted that the DMMs applied for TDR using Stevens-Vitel Hydra Probe 50MHz (SNOTEL) and Stevens Water Hydraprobe Digital Sdi-12 (SCAN) are the polynomial equations whose parameters are set for the inorganic and mineral soils (Seyfried et al., 2005).

Results and Discussion

Evaluation against the Point-Scale Dielectric Constant Data

To assess the effect of OM on the accuracy of soil moisture estimation, our proposed DMM for organic soil was compared with the dielectric constant measured by TDR sensors with other existing mineral and organic models in Table 1 (Fig. 5) (Bircher et al., 2016; Dobson et al., 1985; Miyamoto et al., 2003). In the recent DMM (Park et al., 2017), a 2°C difference during permittivity measurement causes a 0.002 $cm^3\ cm^{-3}$ difference in soil moisture estimation in the 0.35 to 0.40 $cm^3\ cm^{-3}$ range. Furthermore, under wetter conditions with >0.5 $cm^3\ cm^{-3}$, a 2°C difference during permittivity measurement causes a 0.005 $cm^3\ cm^{-3}$ error in the soil moisture estimation using the DMM. The current soil moisture sensors (e.g., SMT-100, Hydra Probe, and 5TE) are measuring soil temperature as well, and for passive microwave estimation of soil moisture the soil temperature needs to be known. That circumvents this problem.

The validation was performed for various levels of OM content (Fig. 5). This validation of the dielectric constant has the advantage that no uncertainty is added by vegetation disturbance, which typically affects TB simulations.

The mineral soil models (the dotted lines) overestimated the dielectric constant compared with the organic models (the solid curves), especially for higher OM content (5–80%). Our findings suggest that, due to the overestimation in calculation of the effective dielectric constant by existing mineral models, the soil moisture measured in organic-rich soils by TDR may be greatly underestimated.

The T_o, R_o, and B_o models were based on the empirical relationship of the dielectric constant with the soil moisture content in organic-rich soil samples. Because the variation in OM was only derived empirically in these three models, they lack a physical basis, which leads to simulation errors. Indeed, their simulation results underestimated the dielectric constant in organic soils (Fig. 6). The M_o model simulated inconsistently because of the high sensitivity of BD to variations in OM. On the contrary, our proposed model showed consistent performance by adjusting the wilting point and porosity according to the OM

Table 2. Input information about the literature-based point samples used for the simulation of the dielectric constant.

Sample	Organic matter	Bulk density	Clay	Silt	Sand	Salinity	Temperature	Sources
	%	g cm^{-3}	%			‰	°C	
Roth et al. (1992), 30 MHz sensor frequency								
Rhodic Ah (J)	2.86	1.15	80	16	4	0	20	Parana, Brazil 0–10 cm
Rhodic Bws (K)	0.74	1.12	81	16	3	0	20	Parana, Brazil 140–160 cm
Podzol (L)	1.93	1.4	2	10	88	0	20	Germany 30–45 cm
Chernozem (M)	3.36	1.26	46	52	2	0	20	Lublin, Poland 0–20 cm
Chromic Luvisol Ah (N)	1	1.46	23	31	46	0	20	Elba, Italy 0–20 cm
Chromic Luvisol Bt (O)	0.21	1.54	34	31	35	0	20	Elba, Italy 150–180 cm
Haplic Luvisol (P)	0.19	1.43	23	75	2	0	20	Germany 90–120 cm
Luvic Calisol Ah (Q)	1.17	1.47	24	26	50	0	20	Elba, Italy 0–20 cm
Luvic Calisol Bt (*R*)	0.63	1.31	46	28	26	0	20	Elba, Italy 80–100 cm
Haplic Ferralsol Ah (S)	1.12	1.44	12	6	82	0	20	Parana, Brazil 0–10 cm
Haplic Ferralsol Bt (T)	0.35	1.55	18	8	72	0	20	Parana, Brazil 120–140 cm
Washed (U)	0	1.72	0	1	99	0	20	Berlin, Germany
C material (V)	0.18	1.67	0	2	98	0	20	Berlin, Germany
Glass beads (W)	0	1.69	0	0	100	0	20	–
Montmorillonite (X)	0.83	1.25	63	36	1	0	20	Poland
Miyamoto et al. (2003), 30 MHz frequency								
Miyamato_2.a Aggregate	25	0.67	2	10	88	0	20	Kyushu Andisol Japan
Miyamato_2.a Crushed	25	0.78	2	10	88	0	20	
Miyamato_2.b Aggregate	25	0.69	2	10	88	0	20	
Miyamato_2.b Crushed	25	0.77	2	10	88	0	20	
Miyamato_2.c Aggregate	25	0.69	2	10	88	0	20	
Miyamato_2.c Crushed	25	0.77	2	10	88	0	20	
Miyamato_2.d Aggregate	25	0.68	2	10	88	0	20	
Miyamato_2.d Crushed	25	0.77	2	10	88	0	20	
Miyamato_3	25	0.69	2	10	88	0	20	
Bircher et al. (2016), 100 MHz frequency								
HOBE_Forest_O1_L	69		23.1	7.8	0.1	0	20	DK, Forest
HOBE_Forest_O2_L	31		61.1	3.3	0	0	20	0–5cm, DK, Forest
FMI_Forest_O_L	36.6		61.7	1.4	0.3	0	20	0–5cm, FMI, Forest
HOBE_Forest_M_L	8		83.9	7.6	0.3	0	20	0–5cm, DK, Forest
FMI_Forest_M_L	15.1		84.8	0.2	0	0	20	0–5cm, FMI, Forest
FMI_Heath_Mç2_L	5		92.4	2.6	0	0	20	0–5cm, FMI, Heath
FMI_Heath_M1_L	6.9		91.5	1.4	0.3	0	20	0–5cm, FMI, Heath
HOBE_Heath_M_F	15.8		84.7	13.9	1.4	0	20	0–5cm, DK, Heath
Wagner et al. (2013), 1 GHz frequency								
	0.6		29.7	50.4	19.9	0.6	20	Thuringia, Germany

content. As the OM content decreased, OM had less impact on the TB simulation and the difference between P and P_o decreased (Fig. 5). That is, P_o converged to the results of the mineral model in low OM.

In general, the effective dielectric constant of organic-rich soils is lower than that of mineral soils across a similar range of soil moisture content. According to Fig. 3, the curve simulated by the OM model (solid red curve) has been further stretched along the *x* axis compared with the mineral model (dotted red curve) owing to the increase in the wilting point and the porosity for high OM content. Consequently, a larger OM induced an increase in the portion of bound water (low dielectric constant) and a reduction in the portion of free water (high dielectric constant) simultaneously. Owing to the reconsideration of the OM effect in the calculation of the effective dielectric constant, P_o showed the best performance against TDR measurements

(RMSE = 4.1 $cm^3\ cm^{-3}$ and absolute bias = 1.9 $cm^3\ cm^{-3}$, which scores approximately half the error of other models) in Fig. 7.

Evaluation Using SMAP Brightness Temperature Data

To investigate the effect of OM in the DMMs on TB simulation (no freezing conditions), a further validation was conducted for a region within the Alaskan boreal area (Yi et al., 2019), which was monitored by the in situ stations from 1 June to 30 Sept. 2015. Via a comparison of TB simulations from the P_oh, P_or, and P models, the OM effect can be investigated because these models only use the input of wilting point and porosity computed from OM according to Table 3 (P_or and P_oh) or USDA soil texture classification without consideration of OM (P model). Our analysis focused on a time series in the central region of Alaska where in situ data are located within satellite footprints (Fig. 8). Our findings suggest that TB simulation can be improved if the temporal variability of soil moisture is properly incorporated into the TB simulation by considering the OM effects on wilting point and porosity in the DMMs.

Table 3. Input information for the simulation of pixel-based brightness temperature from the Harmonized World Soil Database (FAO, 2012) (_h) and the SoilGrid1km database (Hengl et al., 2014) (_r) and vegetation opacity (OP) from MODIS.

Site	Sand_h	Clay_h	OM_h	OM_r	Temporal mean OP
			%		
Aniak	40	21	1.25	40.67	0.27
Canyon Lake	40	21	1.25	51.90	0.24
Checkers Creek	40	21	1.25	38.63	0.22
Hozatka Lake	40	21	1.25	49.97	0.32
Innoko Camp	40	21	1.25	51.71	0.33
Kanaryagak Camp	40	21	1.25	47.76	0.25
Kanuti Lake	40	21	1.25	38.29	0.34
Naknek River	40	21	1.25	40.67	0.24
Nenana	40	21	1.25	36.86	0.51
Tok	40	21	1.25	43.42	0.36
Unalakleet	40	21	1.25	43.42	0.35
Weary Lake	73	9	1.40	36.60	0.36
Anchor River Divide	46	11	4.38	36.33	0.65
Atigun Pass	73	9	1.40	28.33	0.15
Coldfoot	34	18	3.08	38.13	0.26
Eagle Summit	40	21	1.25	40.00	0.32
Exit Glacier	73	9	1.40	0.00	0.44
Gobblers Knob	40	21	1.25	38.70	0.30
Granite Crk	73	9	1.40	35.52	0.51
Imnaviat Creek	73	9	1.40	46.83	0.15
Kelly Station	34	18	3.10	33.70	0.2
Kenai Moose Pens	54	8	4.63	37.46	0.81
Little Chena Ridge	42	22	1.00	47.49	0.43
McNeil River SGS	73	9	1.40	32.71	0.26
Monument Creek	40	21	1.25	32.39	0.39
Moore Creek Bridge	73	9	1.40	39.72	–
Mt. Ryan	40	21	1.25	46.90	0.43
Munson Ridge	42	22	1.00	47.58	0.52
Nuka Glacier	73	9	1.40	0.00	0.44
Point Mackenzie	54	8	4.63	32.23	0.76
Prudhoe Bay	73	18	1.40	29.33	0.24
Rocky Point	40	21	1.25	37.95	0.25
Summit Creek	73	9	1.40	45.89	0.42
Susitna Valley High	54	8	4.63	30.13	0.59
Tokositna Valley	73	9	1.40	37.66	0.41
Upper Tsaina River	73	9	1.40	45.20	0.20

Notwithstanding the scaling issue, the temporal variabilities of the in situ soil moisture and the measured SMAP TB at the 40-km grid scale are well synchronized with respect to daily TB fluctuation (Fig. 8). In this figure, the dynamic of the fluctuation in SMAP TB measurements tends to be smoother than the simulation performed with the point in situ data due to the larger spatial scale of the SMAP measurements than the in situ measurements. We simulated the TB with the various forward models based on the input of in situ soil moisture, and therefore we can directly compare them with the temporal variability of SMAP TB to determine the best performance among them. For example, at Eagle Summit, the TB simulation of the mineral models (P, W, D, and M) showed the significant decrease from dry (Day of the Year [DOY] 200) to wet (DOY 240) by as much as 40 K. During this period, the SMAP TB measurements showed a smaller variability of approximately 20 K. Notably, the issue of the sharp reduction displayed in the mineral models was mitigated in the OM model (P_or) and thus TB simulations were much closer to the SMAP TB measurements. This improvement is also reflected in the ubRMSE values.

Similar patterns for P_or were found in the Little Chena Ridge, Monument Creek, and Munson Ridge samples (Fig. 8). This effect of OM on the TB simulation result (i.e., the mitigation of TB fluctuation with time) was also found in all of the cases presented in Fig. 9, except Innoko Camp. In an oversaturated state (usually >0.48 $cm^3\ cm^{-3}$), the TB simulation did not show significant differences between the OM and mineral models. This effect of OM on TB can be explained by Fig. 3c: the difference in TB between the mineral (the dotted red curve) and the organic model (the solid red curve) initially increased under dry conditions and then started decreasing as soil moisture increased because of the dry porosity. In other words, the uncertainty caused by ignoring OM becomes intensified at a moderate level of soil water content rather than very dry or wet soil. Our analysis proposed that the temporal variation in the microwave TB for OM-rich soils will be lower than that proposed by existing mineral models. For example, in the sample with the highest OM content, Canyon Lake, the variance in TB simulation results among models was clearly observed under moderate levels of soil moisture. In addition, at Canyon Lake, OM became important

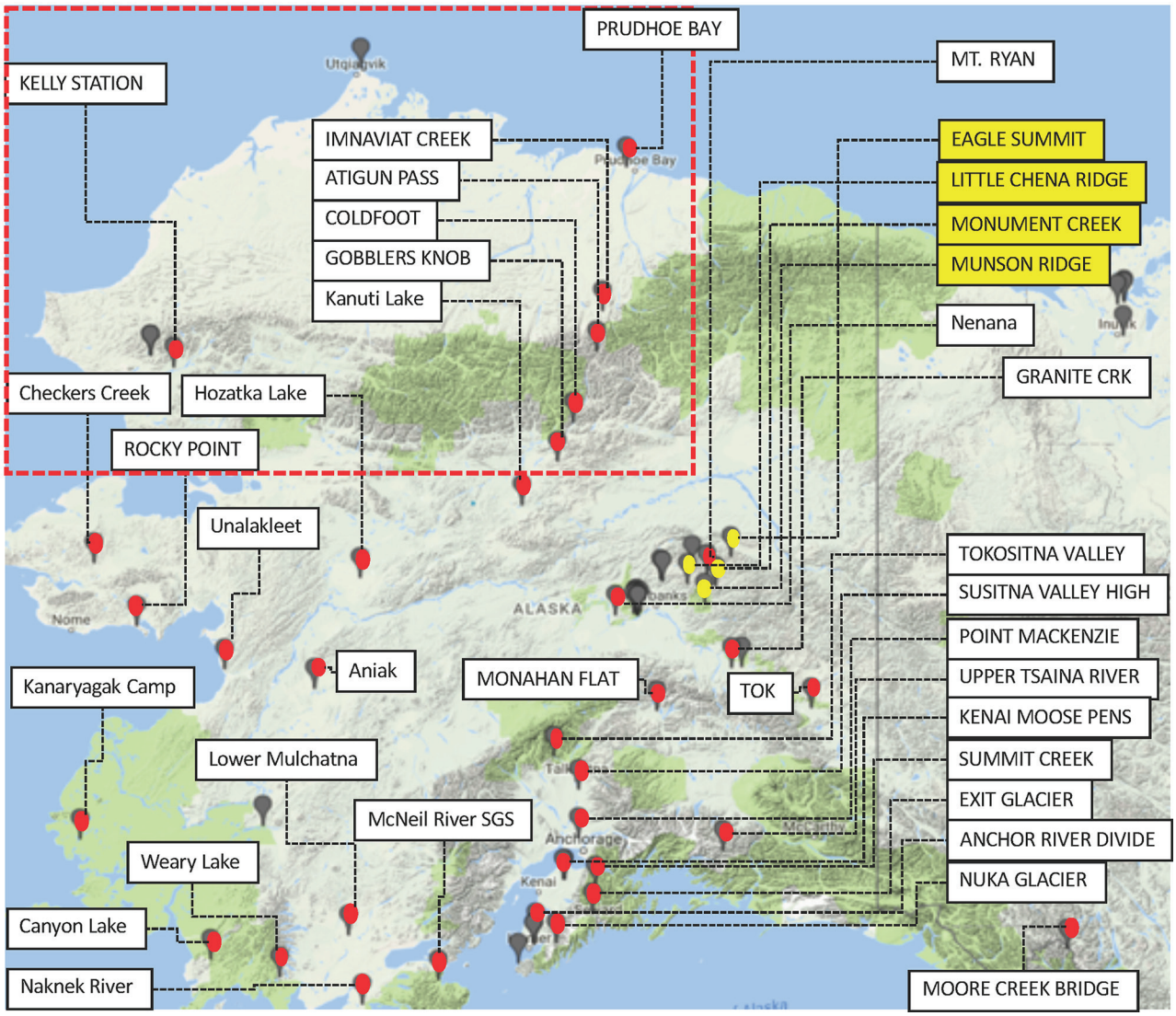

Fig. 4. Sites for evaluation of pixel-based brightness temperature (TB) simulation over boreal forests in artic and alpine tundra, using site information from the International Soil Moisture Network (ISMN). Yellow and red dots show in situ sites where both soil moisture at the 5-cm depth and soil temperature are available for May–November 2015, gray dots are ISMN sites excluded in the experiments due to incomplete in situ measurements. The dashed red box indicates an important site for the reasonable investigation of the organic matter effect on TB because the vegetation disturbance on TB is negligible with the relatively low vegetation optical depth on this area.

when SM was >0.2 cm^3 cm^{-3}. However, when SM reached a saturation point, this difference decreased. In the Innoko Camp sample, the difference in TB between P_or and P was larger within the range of 0.2 to 0.6 cm^3 cm^{-3} and became smaller at values >0.6 cm^3 cm^{-3}. Our results indicate that the uncertainty in TB simulation caused by OM is intensified in the presence of moderate levels of soil moisture. As shown in Fig. 8, the reason for the lower variation originates from the DMM being divided into three phases of SM, which was determined by the wilting point and porosity (related cases in Fig. 9: 1, 2, 4, 5, 7, 8, 14, 15, and 16).

It is also notable that the TB simulation can be affected by OM uncertainty due to vegetation optical depth (VOD of SMAP Level 3 products) in its computation using the MODIS normalized difference vegetation index (NDVI). When there was a significant difference in TB simulations despite the OM and SM content being similar among sites, our analysis showed that this difference was related to the VOD. For example, the difference between the P_or and P_oh models for Nenana (Fig. 9, no. 5) was less significant than that of Canyon Lake (Fig. 9, no. 1). The reason for the weaker effect of OM can be explained by the attenuation of soil emissions by high VOD. A more obvious influence of VOD can be found for the Kenai Moose Pens, where the temporal average of vegetation opacity was very high (0.81). At this site, all the DMMs, including the mineral models, had negligible differences in TB simulation. On the other hand, at Imnaviat Creek, where the vegetation opacity was as low as 0.15, the improvement in the estimation of TB was more prominent by incorporating OM (P_o).

In Fig. 10, the DMMs that included the wilting point and porosity as a function of OM produced the most accurate TB

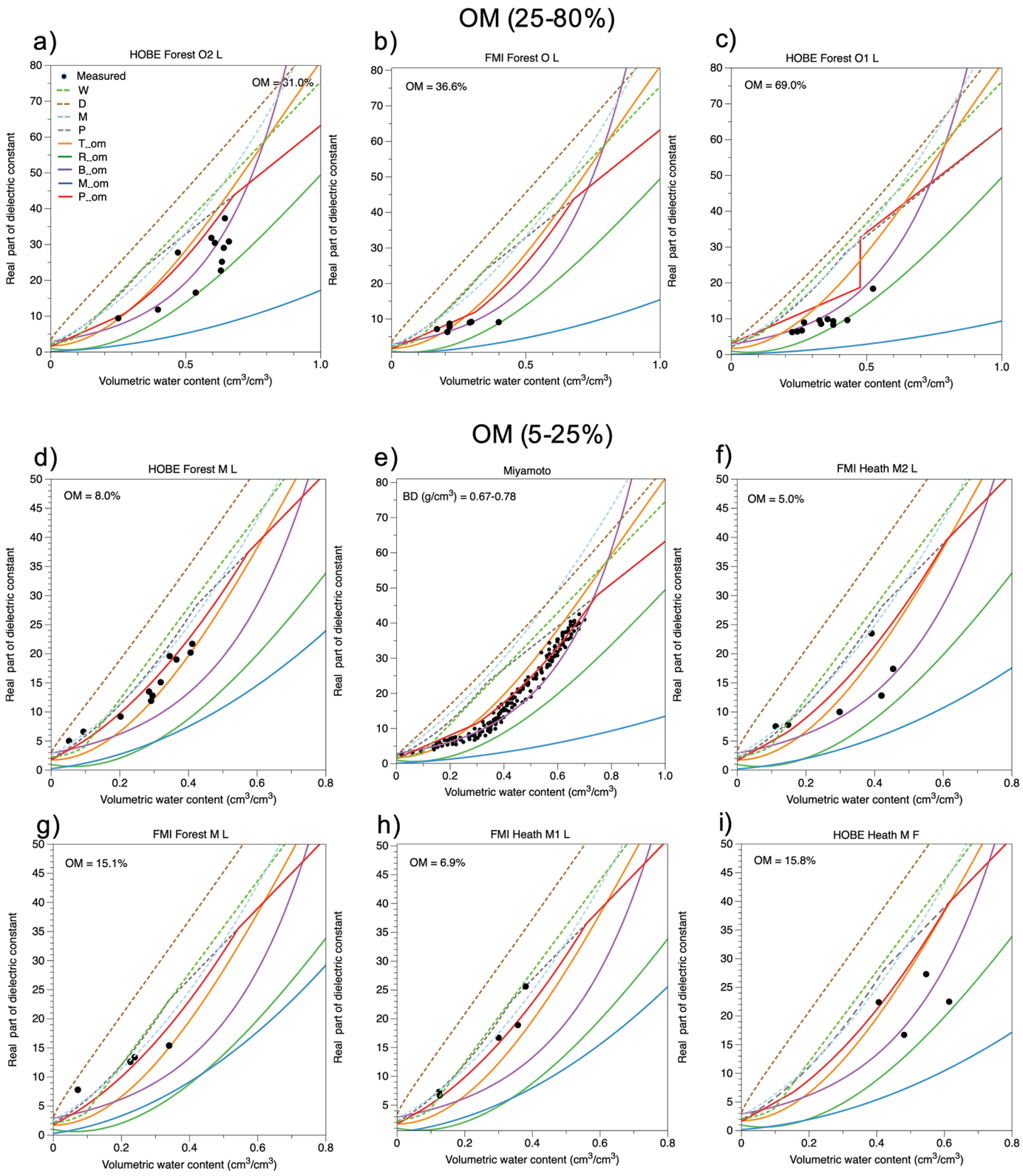

Fig. 5a. Comparison of the dielectric constant simulation by dielectric mixing models (DMMs) for mineral soil (dashed curves) and organic soil (solid curves) for a range of organic matter (OM) against measurements (dots). The DMMs included Wang and Schmugge (1980) (W), Dobson et al. (1985) (D), Mironov et al. (2009) (M), Park et al. (2017) (P), Topp et al. (1980) (T_o), Roth et al. (1992) (R_o), Mironov and Savin (2015) (M_o), Bircher et al. (2016) (B_o), and Park et al. (2017) (P_o) using Eq.[1] and [2]; "o" indicates organic soil and the accompanying number is the sample number from a particular site; L refers to a sample measured in the laboratory.

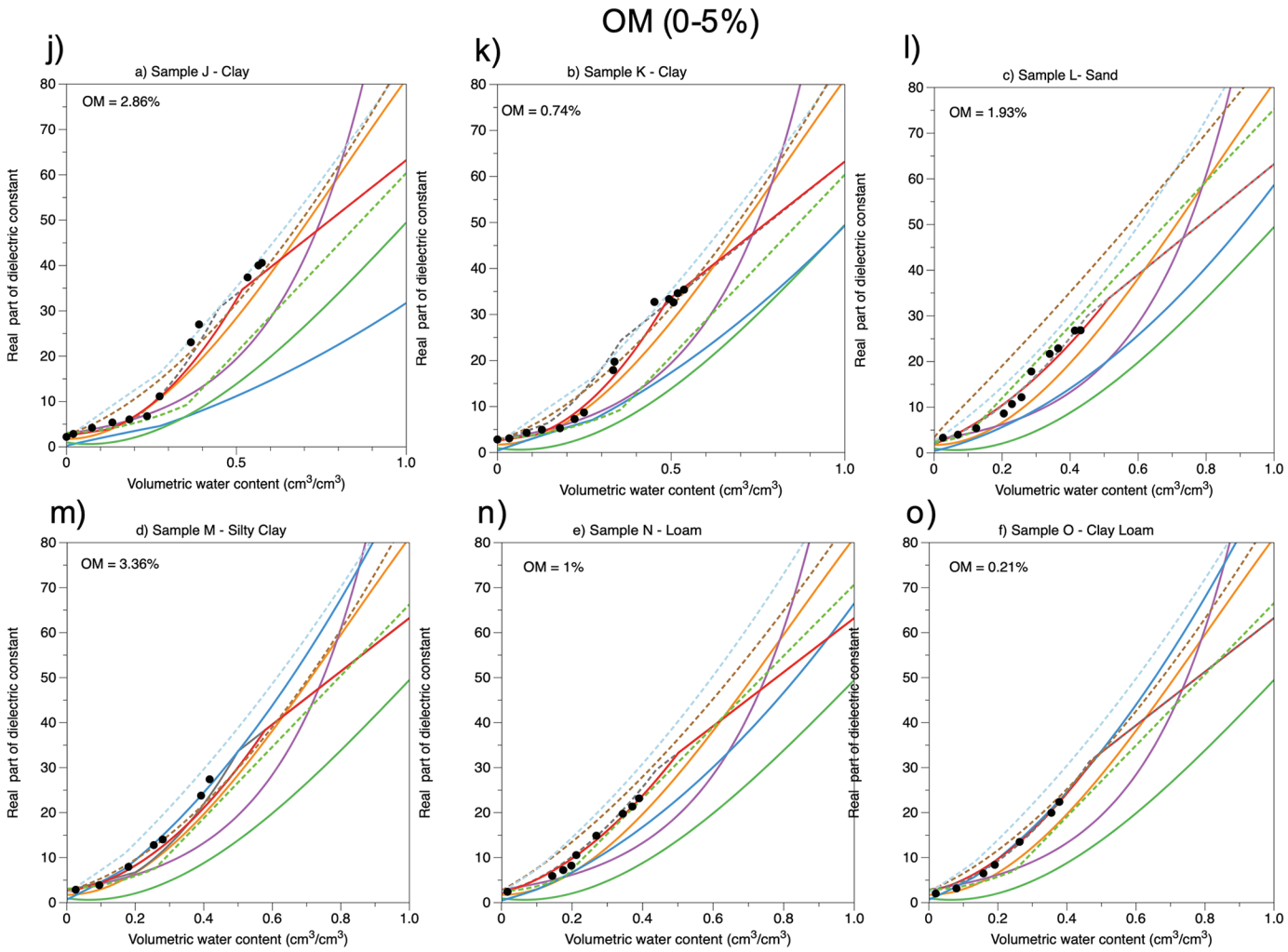

Fig. 5b. Comparison of the dielectric constant simulation by dielectric mixing models (DMMs) for mineral soil (dashed curves) and organic soil (solid curves) for a range of organic matter (OM) against measurements (dots). The DMMs included Wang and Schmugge (1980) (W), Dobson et al. (1985) (D), Mironov et al. (2009) (M), Park et al. (2017) (P), Topp et al. (1980) (T_o), Roth et al. (1992) (R_o), Mironov and Savin (2015) (M_o), Bircher et al. (2016) (B_o), and Park et al. (2017) (P_o) using Eq.[1] and [2]; "o" indicates organic soil and the accompanying number is the sample number from a particular site; L refers to a sample measured in the laboratory.

predictions compared with the SMAP TB measurements, thus overcoming the underestimation produced by other models. In particular, our proposed DMMs (P_or or P_oh) made the most accurate prediction compared with SMAP TB in the boreal forest regions in terms of bias, ubRMSE, and correlation coefficient. Based on rank validation, P_o also performed better than P_oh and the other OM and mineral models. The TB simulation over Alaska with the input of TDR SM is from no-OM DMMs, as mentioned above. This will exacerbate the positive bias and mitigate negative bias in the comparison. This effect might be reflected as a benefit in the bias score, especially in the performance of mineral DMMs such as P, W, D, and M under the uncertainty of VOD, soil roughness parameter, and standing water fraction because the SM as an input of the RTM is provided based on a TDR instrument with the mineral model for SNOTEL and SCAN.

Investigation of SMAP Soil Moisture Products

To investigate the current SMAP soil moisture products of Level 3 (no OM consideration within the RTM) and Level 4 (same RTM but combined with data assimilation containing hydraulic properties including OM), we compared the SMAP products within the red box in Fig. 11 (high OM content over northwestern Alaska). This region allows a proper investigation of OM effect because OM is very high (Fig. 11a) without strong vegetation disturbance (Fig. 11b). Across this region at that period, the measured surface soil moisture from ISMN sites within the red box in Fig. 4 ranged from 0.2 to 0.3 cm^3 cm^{-3} (see the soil moisture time series, 11–14, in Fig. 9). However, the Level 3 SMAP soil moisture retrieved by Single Channel Algorithm V-pol, which adapted the Mironov model (Mironov et al., 2009) (SM1 in Fig. 11) over the Alaska region has much lower values, <0.1 cm^3 cm^{-3} as shown in Fig. 11c, because SM1 is estimated

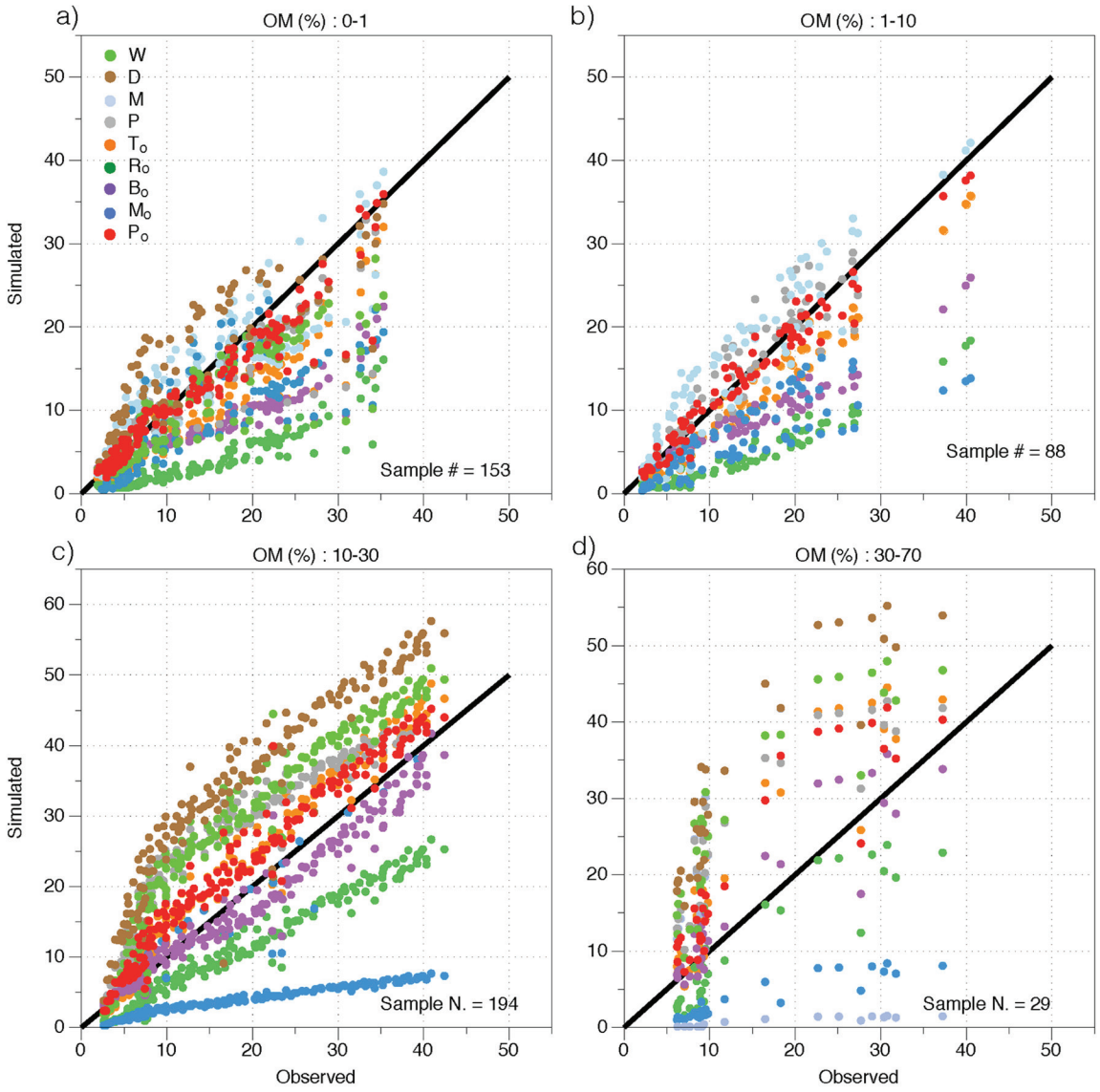

Fig. 6. Scatterplots of observed and simulated dielectric constants classified by the amount of organic matter (OM): (a) 0 to 1%, (b) 1 to 10%, (c) 10 to 30%, (d) 30 to 70%. The various mixing models included Wang and Schmugge (1980) (W), Dobson et al. (1985) (D), Mironov et al. (2009) (M), Park et al. (2017) (P), Topp et al. (1980) (T_o), Roth et al. (1992) (R_o), Mironov and Savin (2015) (M_o), Bircher et al. (2016) (B_o), and Park et al. (2017) (P_o).

without consideration of OM in the RTM, as illustrated in Fig. 12. On the other hand, the soil moisture of SMAP Level 4 (SM2) is overestimated (0.4–0.5 cm^3 cm^{-3}). Because one of the determining factors in the SM estimation from TB over this region (low vegetation) is the high OM content, it is reasonable to suspect that the OM effect is slightly overpowered in the SM2 (or the input of OM is too high) during the data assimilation. In our study, we simulated TB with the input of the SM measurements of the ISMN, which ranged between SM1 and SM2, and the OM-considered DMM. Then we validated the result of the TB simulation with the SMAP TB. The analysis of the bias and RMSE showed that the new approach is better than the Mironov model, which is used for the estimation of SM1 and SM2 via the current SMAP RTM.

Summary and Conclusion

In this study, we developed a DMM to account for the effect of soil OM on microwave signals explicitly. Our proposed model is an extension of the previous work of Park et al. (2017) to include variations of OM via adjusted soil hydraulic properties into a DMM and forward RTM. To validate the proposed model, simulations of the dielectric constant and TB were compared with in situ TDR measurements and remotely sensed SMAP TB and soil moisture products.

For a wide range of OM content, the developed model performed better than existing empirical calibration models for SM (Bircher et al., 2016; Roth et al., 1992; Topp et al., 1980) and semiempirical DMMs (Dobson et al., 1985; Mironov et al., 2009; Wang and Schmugge, 1980). The TB simulated by M_oh was

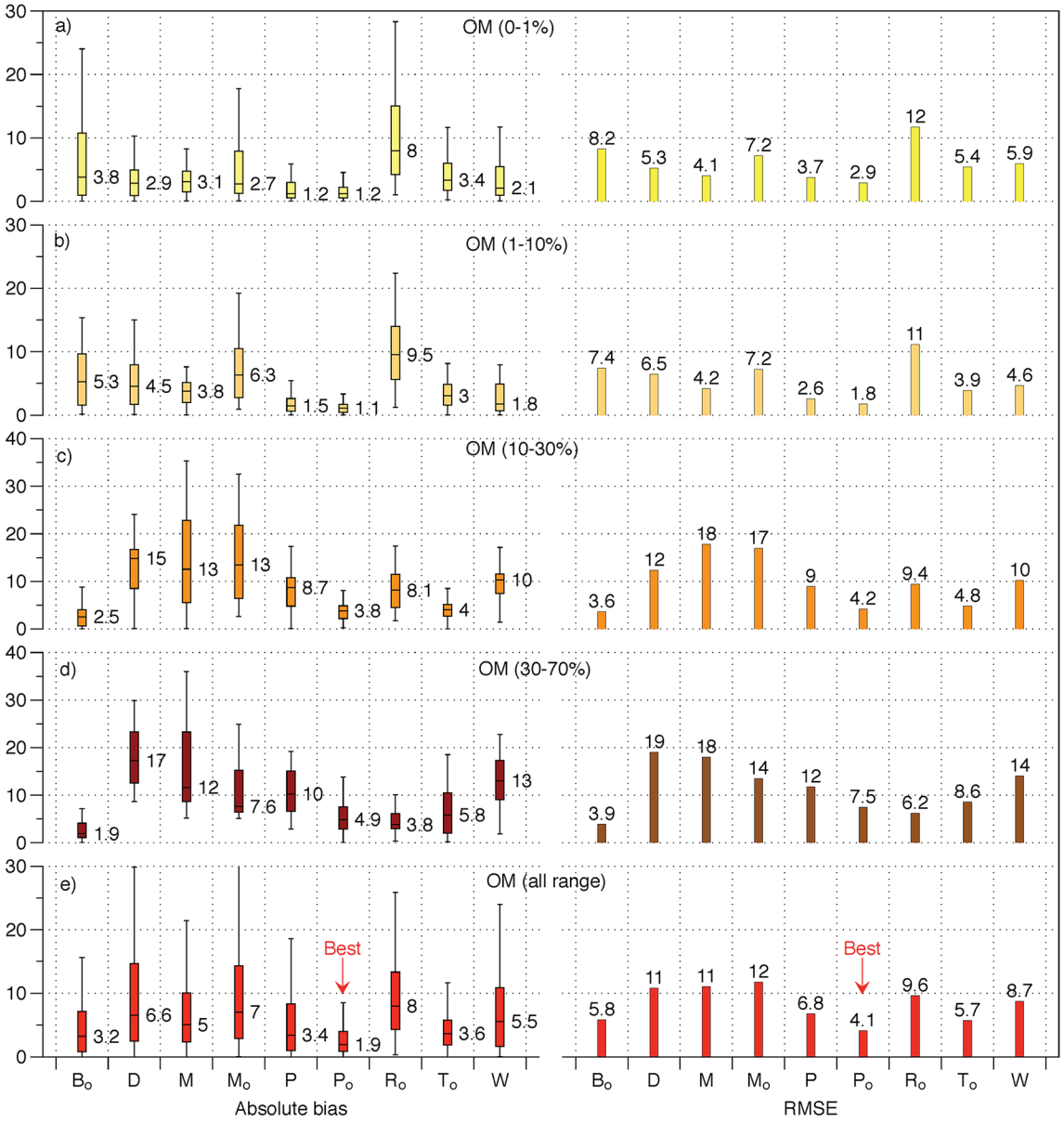

Fig. 7. Absolute bias ($cm^3\ cm^{-3}$) and RMSE ($cm^3\ cm^{-3}$) between point-based measurements and simulations of dielectric constants using various dielectric mixing models: Bircher et al. (2016) (B_o), Dobson et al. (1985) (D), Mironov et al. (2009) (M), Mironov and Savin (2015) (M_o), Park et al. (2017) (P) and as proposed in this study (P_o), Roth et al. (1992) (R_o), Topp et al. (1980) (T_o), and Wang and Schmugge (1980) (W).

unstable with time, while our new model uses OM to update the wilting point and porosity directly and reproduced the observed temporal variability in SMAP TB more realistically. Our findings indicate that the minor uncertainty in relation to OM within the BD term can lead to substantial underestimation of the effective dielectric constant and accordingly overestimation of TB.

The proposed model is applicable to both mineral and organic-rich soils without changes to the model structure because the OM is accounted for in the wilting point and porosity, which are parameters of the DMM. In addition, our model can be used in a wide range of OM concentrations, thereby providing a relatively simple and physically plausible model for improved remotely sensed soil moisture retrievals from, for example, the SMAP, SMOS, and AMSR2 missions. In this study, we found that current SMAP soil moisture products of Level 3 and 4 suffer from underestimation and overestimation issues, respectively. Our model can be used for the soil moisture retrieval algorithm (SMAP Level 3) to resolve the underestimation issue in the soil moisture estimation in high-OM regions. There are some recent SMOS (Kerr et al., 2010) and SMAP (Reichle et al., 2015, 2016, 2017) assimilation studies that account for OM in both the land surface and DMM via updated soil hydraulic properties. However, in this study, we found that it tends to overestimate soil moisture over a high-OM surface. The proposed approach can be applied for forward modeling in TB data assimilation systems (SMAP Level 4) to mitigate this issue.

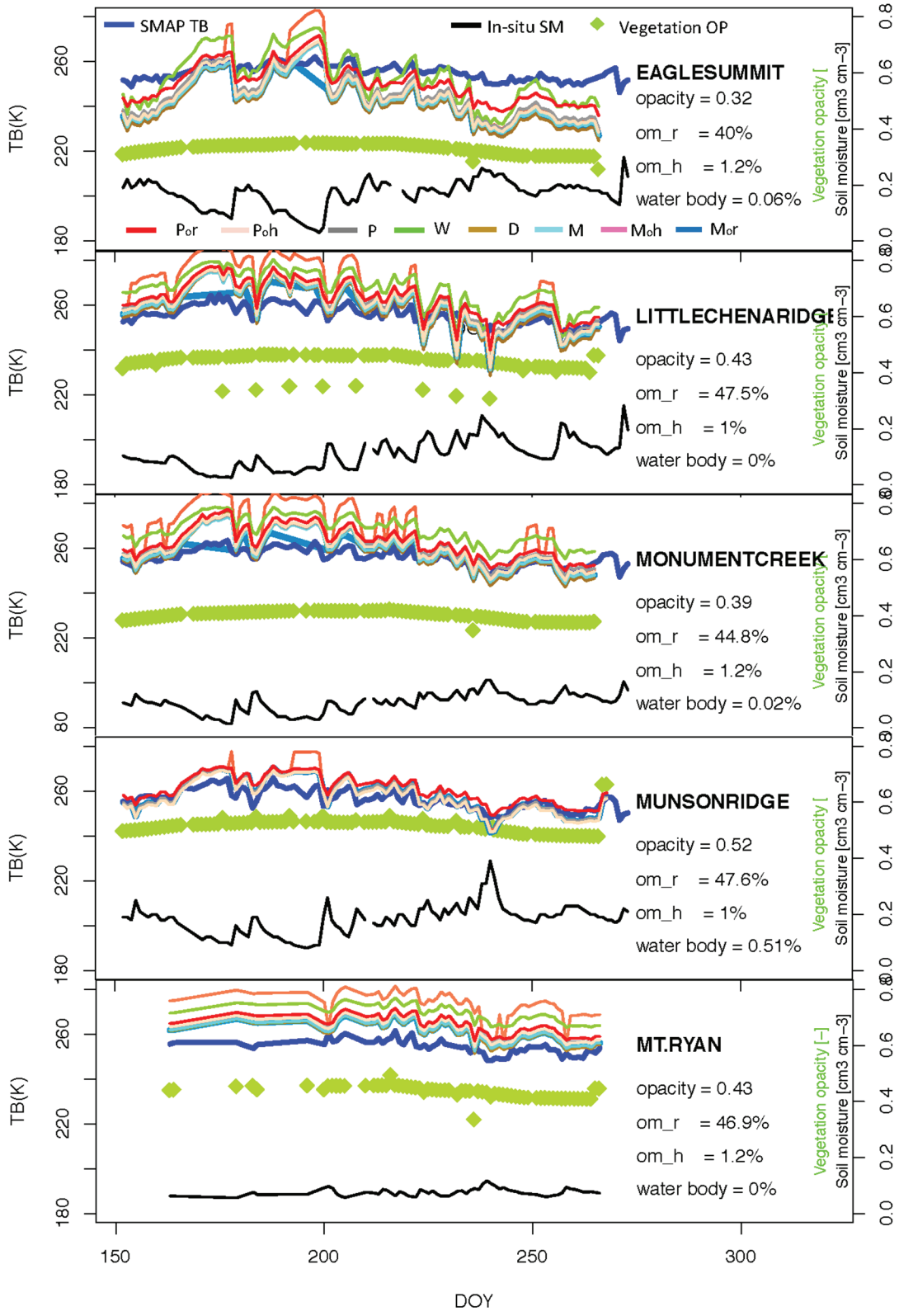

Fig. 8. Evaluation of brightness temperature (TB) simulations for the yellow dots in Fig. 4 using SMAP TB measurements (blue lines), in situ soil moisture (SM) content (black lines), and vegetation opacity (thick green dots) from MODIS; and dielectric mixing models (Park et al., 2017) with wilting point (Eq. [1]) functions and organic matter (OM) input from the SoilGrid1km database (Hengl et al., 2014) (P_or), with wilting point (Jin et al., 2017) and porosity (Wösten et al., 1999) functions and OM input from the Harmonized World Soil Database (FAO, 2012) (P_oh), with wilting point and porosity classified by USDA soil classification (P), Wang and Schmugge (1980) (W), Dobson et al. (1985) (D), and Mironov et al. (2009) (M) with OM input from the Harmonized World Soil Database (FAO, 2012) (M_oh) and the SoilGrid1km database (Hengl et al., 2014) (M_or).

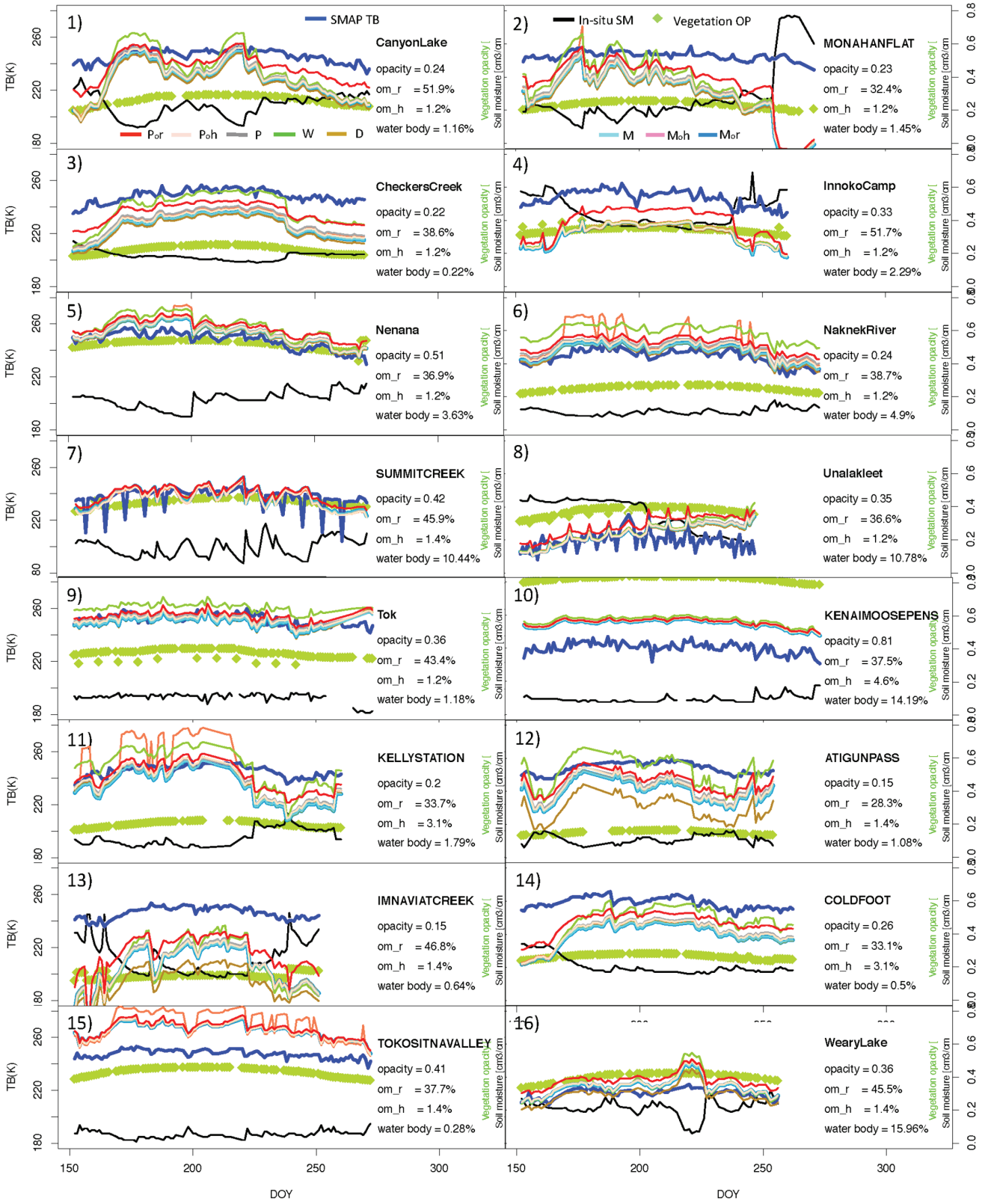

Fig. 9. Evaluation of brightness temperature (TB) simulations for other International Soil Moisture Network sites (red dots in Fig. 4) using SMAP TB measurements (blue lines), in situ soil moisture (SM) content (black lines), and vegetation opacity (thick green dots) from MODIS; and dielectric mixing models (Park et al., 2017) with wilting point (Eq. [1]) functions and organic matter (OM) input from the SoilGrid1km database (Hengl et al., 2014) ($P_o r$), with wilting point (Jin et al., 2017) and porosity (Wösten et al., 1999) functions and OM input from the Harmonized World Soil Database (FAO, 2012) ($P_o h$), with wilting point and porosity classified by USDA soil classification (P), Wang and Schmugge (1980) (W), Dobson et al. (1985) (D), and Mironov et al. (2009) (M) with OM input from the Harmonized World Soil Database (FAO, 2012) ($M_o h$) and the SoilGrid1km database (Hengl et al., 2014) ($M_o r$).

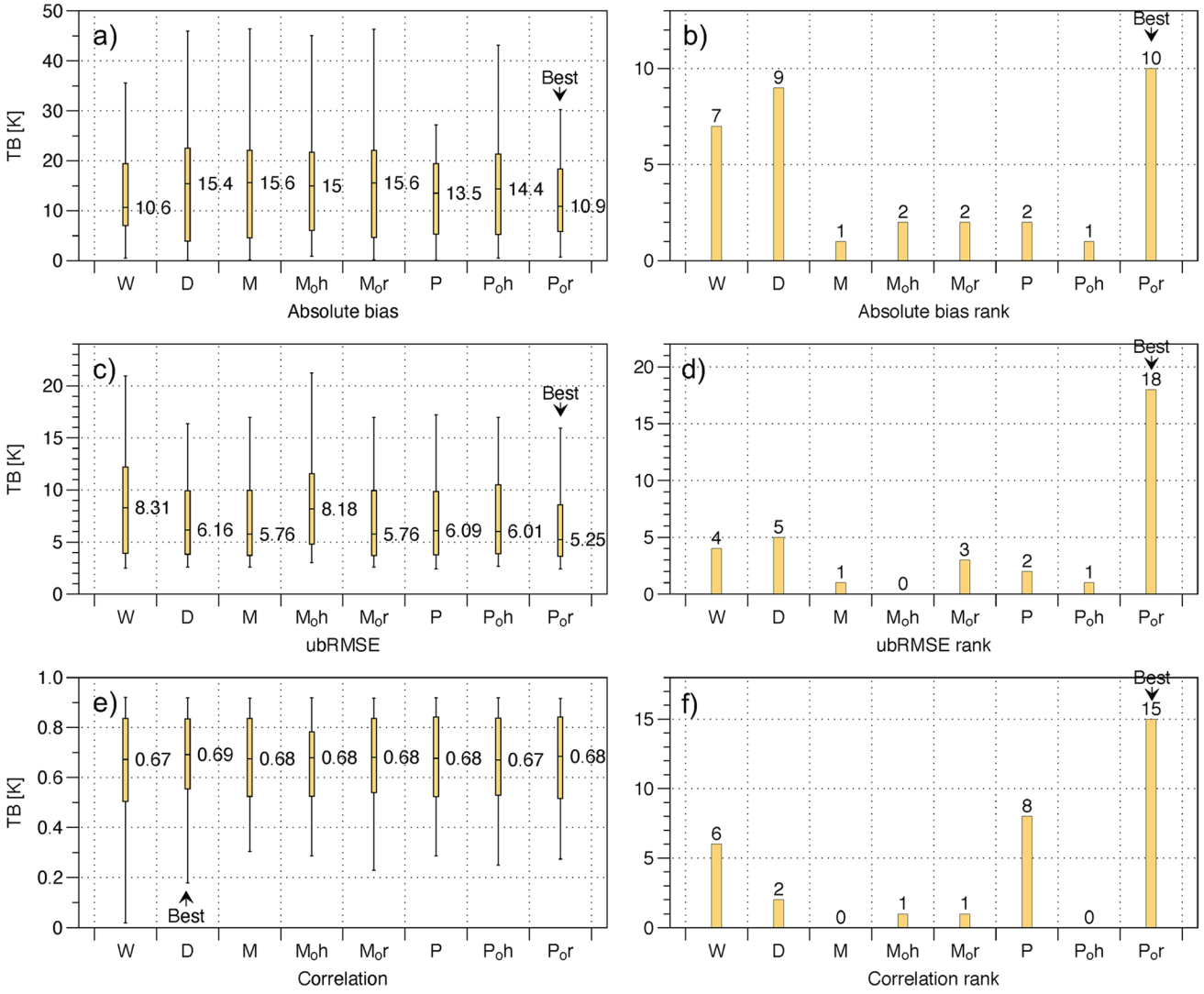

Fig. 10. Spatially averaged brightness temperature (Tb) evaluation scores for the 35 International Soil Moisture Network sites in Table 3, calculated for the period from 1 June to 30 Sept. 2015 (left), and the number of counts for first rank among the tested models (right). The models included Wang and Schmugge (1980) (W), Dobson et al. (1985) (D), Mironov et al. (2009) (M) and with organic matter (OM) input from the Harmonized World Soil Database (FAO, 2012) (M_oh) and the SoilGrid1km database (Hengl et al., 2014) (M_or), and (Park et al., 2017) with wilting point and porosity classified by USDA soil classification (P) and with wilting point (Eq. [1]) functions and OM input from the SoilGrid1km database (P_or) or with wilting point (Jin et al., 2017) and porosity (Wösten et al., 1999) functions and OM input from the Harmonized World Soil Database (P_oh).

Appendix

Vegetation opacity τ used in SMAP retrievals is a MODIS-based product [MODIS 1000m MOD13A2(V005) NDVI (Chan et al., 2013)] based on the volumetric water content–NDVI relationship (Jackson et al., 2004; O'Neill et al., 2015) and the τ–volumetric water content relationship (Jackson and Schmugge, 1991; Van de Griend and Wigneron, 2004) as shown in Eq. [8], [9], and [10], respectively:

$$\mathrm{NDVI}=\frac{R_{\mathrm{NIR}}-R_{\mathrm{RED}}}{R_{\mathrm{NIR}}+R_{\mathrm{RED}}} \quad [8]$$

where R_{NIR} and R_{RED} are the radiance at 0.78 to 0.90 and 0.63 to 0.69 μm, respectively,

$$\mathrm{VWC}=a_0+a_1\mathrm{NDVI}^1+a_2\mathrm{NDVI}^2+a_3\mathrm{NDVI}^3+a_4\mathrm{NDVI}^4+a_5\mathrm{NDVI}^5 \quad [9]$$

where a_{0-5} are 0.13, −1.24, 6.87, −11.41, 7.63, and 0 for C_3 plants and −2.822, 30.699, −138.93, 347.96, −417.46, and 192.64 for C_4 plants, and

$$\tau=b\,\mathrm{VWC} \quad [10]$$

The linearly proportional factor b is determined according to the structure of the canopy (Jackson and Schmugge, 1991). This value can be estimated from the NDVI (O'Neill et al., 2015). Then the transmissivity of the canopy (t) is computed using τ and the incident angle θ:

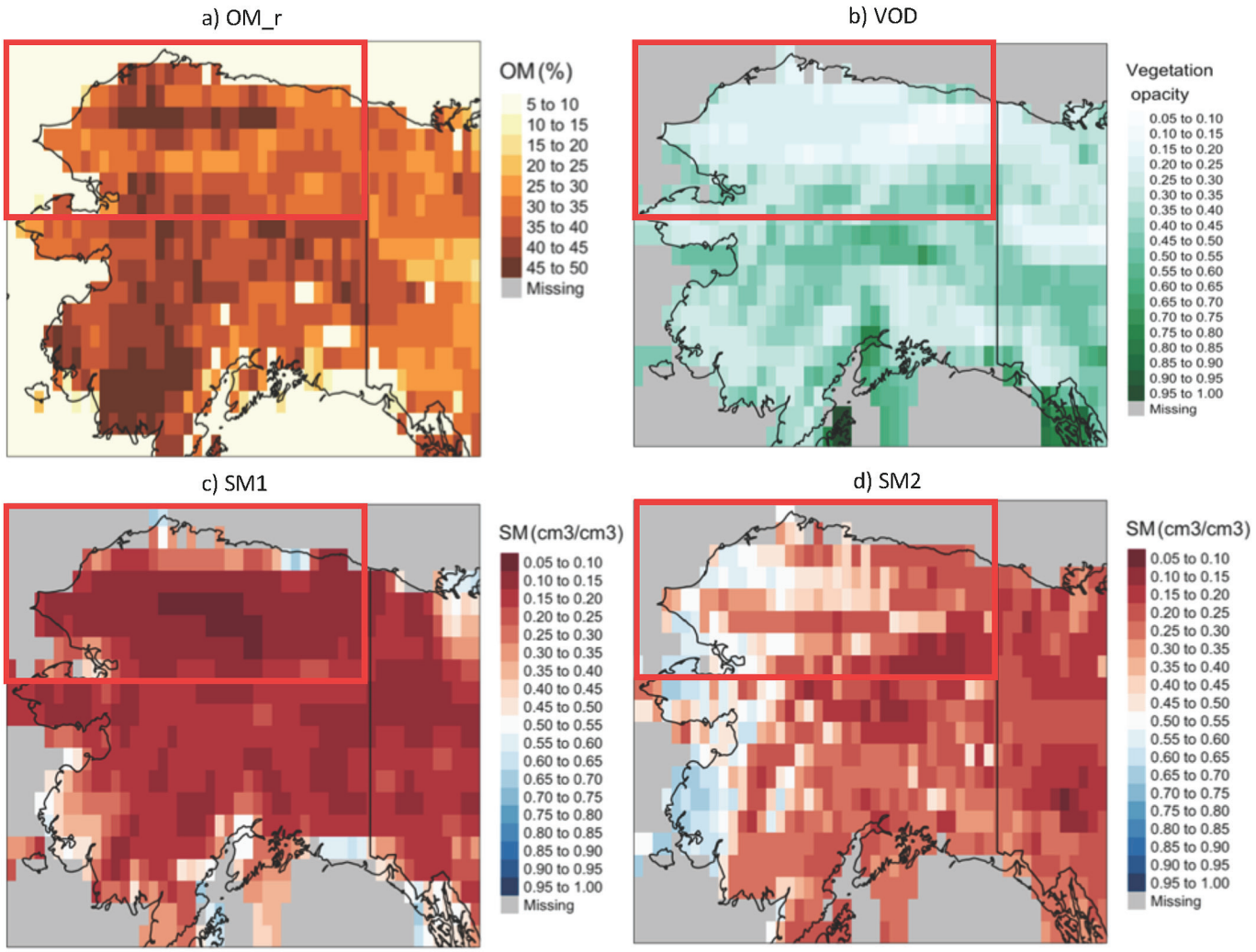

Fig. 11. Investigation of SMAP soil moisture products: (a) organic matter (OM) from the SoilGrids1km dataset (Hengl et al., 2014), (b) SMAP Level 3 vegetation optical depth (VOD) based on MODIS normalized difference vegetation index measurements, (c) SMAP soil moisture (SM) estimation from Level 3 (SM1) without an OM effect, and (d) SMAP SM estimation from Level 4 (SM2) with OM effect reflected via data over Alaska at 6 AM on 1 Aug. 2015 UTC; the red box indicates the region where the OM effect appears well on SMAP SM products owing to higher OM but less VOD disturbance.

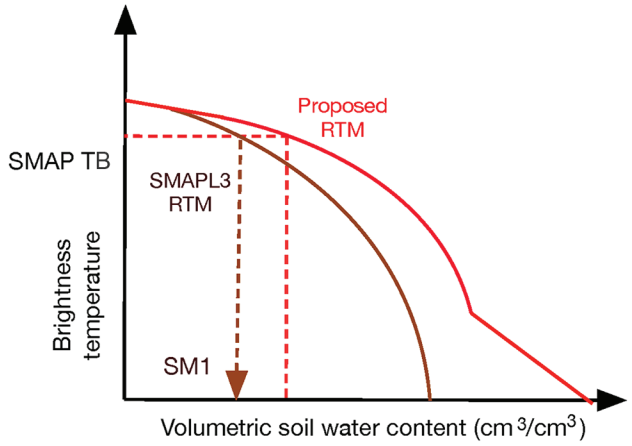

Fig. 12. Comparison of the radiative transfer model (RTM) including the proposed dielectric mixing model with the approaches applied in the current SMAP Levels 3 and 4 for soil moisture (SM) estimation.

$$t = \exp\left(\frac{-\tau}{\cos\theta}\right) \quad [11]$$

The TB at vertical and horizontal polarization within a SMAP grid cell is determined according to

$$\mathrm{TB}_{\mathrm{v,h}} = (1-f_{\mathrm{w}})\left[(1-t)(1+tr_{\mathrm{v,h}})T_{\mathrm{c}} + t(1-r_{\mathrm{v,h}})T_{\mathrm{s}}\right] + f_{\mathrm{w}}(1-\mathrm{rw}_{\mathrm{v,h}})T_{\mathrm{s}} \quad [12]$$

where T_{s} is surface temperature, T_{c} is canopy temperature (assumed to be the same as T_{s} in this study), f_{w} is the water fraction within a SMAP grid (MODIS MOD44W [Chan, 2013; Chan et al., 2016]), and rw_{h} and rw_{v} are the horizontally and vertically polarized reflectivity of the water body, which are 0.68 and 0.52, respectively.

Acknowledgments

This study was funded by the European Commission Horizon 2020 Program via the ERA-PLANET/GEOEssential (Grant Agreement no. 689443) project, the German Research Foundation (DFG) under Grant JO 1262/2-1, the MIT–Germany Seed Fund "Global Water Cycle and Environmental Monitoring using Active and Passive Satellite-based Microwave Instruments," the Research Foundation–Flanders (FWO-1512817N), a National Research Foundation of Korea grant funded by the Korean government (MSIT) (no. NRF-2018R1A5A1024958 and PN19081), and the Korea Meteorological Administration Research and Development Program under Grant KMI2018-0351, "Development of Climate Prediction System" under Grant (1365003054).

References

Babaeian, E., M. Sadeghi, S.B. Jones, C. Montzka, H. Vereecken, and M. Tuller. 2019. Ground, proximal and satellite remote sensing of soil moisture. Rev. Geophys. 57:530–616. doi:10.1029/2018RG000618

Bircher, S., M. Andreasen, J. Vuollet, J. Vehviläinen, K. Rautiainen, F. Jonard, et al. 2016. Soil moisture sensor calibration for organic soil surface layers. Geosci. Instrum., Methods Data Syst. 5:109–125. doi:10.5194/gi-5-109-2016

Bircher, S., N. Skou, K.H. Jensen, J. Walker, and L. Rasmussen. 2012. A soil moisture and temperature network for SMOS validation in western Denmark. Hydrol. Earth Syst. Sci. 16:1445–1463. doi:10.5194/hess-16-1445-2012

Chan, C.Y., and R.J. Knight. 1999. Determining water content and saturation from dielectric measurements in layered materials. Water Resour. Res. 35:85–93. doi:10.1029/1998WR900039

Chan, S. 2013. SMAP ancillary data report on static water fraction. Jet Propulsion Lab., California Inst. Technol., Pasadena.

Chan, S., R. Bindlish, P. O'Neill, T. Jackson, E. Njoku, S. Dunbar, et al. 2018. Development and assessment of the SMAP enhanced passive soil moisture product. Remote Sens. Environ. 204:931–941. doi:10.1016/j.rse.2017.08.025

Chan, S., R. Bindlish, R. Hunt, E. Njoku, J. Kimball, and T. Jackson. 2013. Vegetation water content. Ancillary data report. Jet Propulsion Lab., California Inst. Technol., Pasadena.

Chan, S.K., R. Bindlish, P.E. O'Neill, E. Njoku, T. Jackson, A. Colliander, et al. 2016. Assessment of the SMAP passive soil moisture product. IEEE Trans. Geosci. Remote Sens. 54:4994–5007. doi:10.1109/TGRS.2016.2561938

Choudhury, B., T.J. Schmugge, A. Chang, and R. Newton. 1979. Effect of surface roughness on the microwave emission from soils. J. Geophys. Res. Oceans 84:5699–5706. doi:10.1029/JC084iC09p05699

De Lannoy, G.J., R.D. Koster, R.H. Reichle, S.P. Mahanama, and Q. Liu. 2014. An updated treatment of soil texture and associated hydraulic properties in a global land modeling system. J. Adv. Model. Earth Syst. 6:957–979.

De Lannoy, G.J., and R.H. Reichle. 2016a. Global assimilation of multiangle and multipolarization SMOS brightness temperature observations into the GEOS-5 catchment land surface model for soil moisture estimation. J. Hydrometeorol. 17:669–691.

De Lannoy, G.J., and R.H. Reichle. 2016b. Assimilation of SMOS brightness temperatures or soil moisture retrievals into a land surface model. Hydrol. Earth Syst. Sci. 20:4895–4911.

Dobson, M.C., F.T. Ulaby, M.T. Hallikainen, and M.A. Elrayes. 1985. Microwave dielectric behavior of wet soil: 2. Dielectric mixing models. IEEE Trans. Geosci. Remote Sens. GE-23:35–46. doi:10.1109/TGRS.1985.289498

Dorigo, W., A. Xaver, M. Vreugdenhil, A. Gruber, A. Hegyiova, A. Sanchis-Dufau, et al. 2013. Global automated quality control of in situ soil moisture data from the International Soil Moisture Network. Vadose Zone J. 12(3). doi:10.2136/vzj2012.0097

Entekhabi, D., E.G. Njoku, P.E. O'Neill, K.H. Kellogg, W.T. Crow, W.N. Edelstein, et al. 2010. The Soil Moisture Active Passive (SMAP) mission. Proc. IEEE 98:704–716. doi:10.1109/JPROC.2010.2043918

Escorihuela, M.J., Y.H. Kerr, P. de Rosnay, J.-P. Wigneron, J.-C. Calvet, and F. Lemaitre. 2007. A simple model of the bare soil microwave emission at L-band. IEEE Trans. Geosci. Remote Sens. 45:1978–1987. doi:10.1109/TGRS.2007.894935

FAO. 2012. Harmonized world soil database (Version 1.2). FAO, Rome. http://www.fao.org/soils-portal/soil-survey/soil-maps-and-databases/harmonized-world-soil-database-v12/en/

Gupta, S., and W. Larson. 1979. Estimating soil water retention characteristics from particle size distribution, organic matter percent, and bulk density. Water Resour. Res. 15:1633–1635. doi:10.1029/WR015i006p01633

Hallikainen, M.T., F.T. Ulaby, M.C. Dobson, M.A. Elrayes, and L.K. Wu. 1985. Microwave dielectric behavior of wet soil: 1. Empirical models and experimental observations. IEEE Trans. Geosci, Remote Sens. GE-23:25–34. doi:10.1109/TGRS.1985.289497

Hengl, T., J.M. de Jesus, R.A. MacMillan, N.H. Batjes, G.B. Heuvelink, E. Ribeiro, et al. 2014. SoilGrids1km: Global soil information based on automated mapping. PLoS One 9:e105992. doi:10.1371/journal.pone.0105992

Jackson, T., and T. Schmugge. 1991. Vegetation effects on the microwave emission of soils. Remote Sens. Environ. 36:203–212. doi:10.1016/0034-4257(91)90057-D

Jackson, T.J., D. Chen, M. Cosh, F. Li, M. Anderson, C. Walthall, et al. 2004. Vegetation water content mapping using Landsat data derived normalized difference water index for corn and soybeans. Remote Sens. Environ. 92:475–482. doi:10.1016/j.rse.2003.10.021

Jin, M., X. Zheng, T. Jiang, X. Li, X.-J. Li, and K. Zhao. 2017. Evaluation and improvement of SMOS and SMAP soil moisture products for soils with high organic matter over a forested area in Northeast China. Remote Sens. 9:387. doi:10.3390/rs9040387

Jonard, F., L. Weihermuller, K.Z. Jadoon, M. Schwank, H. Vereecken, and S. Lambot. 2011. Mapping field-scale soil moisture with L-band radiometer and ground-penetrating radar over bare soil. IEEE Trans. Geosci Remote Sens. 49:2863–2875. doi:10.1109/TGRS.2011.2114890

Jones, L.A., J.S. Kimball, K.C. McDonald, S.T.K. Chan, E.G. Njoku, and W.C. Oechel. 2007. Satellite microwave remote sensing of boreal and arctic soil temperatures from AMSR-E. IEEE Trans. Geosci Remote Sens. 45:2004–2018. doi:10.1109/TGRS.2007.898436

Jones, S.B., and S.P. Friedman. 2000. Particle shape effects on the effective permittivity of anisotropic or isotropic media consisting of aligned or randomly oriented ellipsoidal particles. Water Resour. Res. 36:2821–2833. doi:10.1029/2000WR900198

Kellner, E., and L.-C. Lundin. 2001. Calibration of time domain reflectometry for water content in peat soil. Nord. Hydrol. 32:315–332. doi:10.2166/nh.2001.0018

Kerr, Y.H., P. Waldteufel, J.-P. Wigneron, S. Delwart, F. Cabot, J. Boutin, et al. 2010. The SMOS mission: New tool for monitoring key elements of the global water cycle. Proc. IEEE 98:666–687. doi:10.1109/JPROC.2010.2043032

Klotzsche, A., F. Jonard, M. Looms, J. van der Kruk, and J. Huisman. 2018. Measuring soil water content with ground penetrating radar: A decade of progress. Vadose Zone J. 17:180052. doi:10.2136/vzj2018.03.0052

Lambot, S., M. Antoine, I. van den Bosch, E. Slob, and M. Vanclooster. 2004a. Electromagnetic inversion of GPR signals and subsequent hydrodynamic inversion to estimate effective vadose zone hydraulic properties. Vadose Zone J. 3:1072–1081. doi:10.2136/vzj2004.1072

Lambot, S., E. Slob, I. van den Bosch, B. Stockbroeckx, B. Scheers, and M. Vanclooster. 2004b. Estimating soil electric properties from monostatic ground-penetrating radar signal inversion in the frequency domain. Water Resour. Res. 40:W04205. doi:10.1029/2003WR002095

Lambot, S., E.C. Slob, I. van den Bosch, B. Stockbroeckx, and M. Vanclooster. 2004c. Modeling of ground-penetrating radar for accurate characterization of subsurface electric properties. IEEE Trans. Geosci. Remote Sens. 42:2555–2568. doi:10.1109/TGRS.2004.834800

Mironov, V., and I. Savin. 2015. A temperature-dependent multi-relaxation spectroscopic dielectric model for thawed and frozen organic soil at 0.05–15 GHz. Phys. Chem. Earth, Parts A/B/C 83–84:57–64. doi:10.1016/j.pce.2015.02.011

Mironov, V.L., R.D. De Roo, and I.V. Savin. 2010. Temperature-dependable microwave dielectric model for an Arctic soil. IEEE Trans. Geosci Remote Sens. 48:2544–2556. doi:10.1109/TGRS.2010.2040034

Mironov, V.L., L. Kosolapova, I.V. Savin, and K.V. Muzalevskiy. 2015. Temperature dependent dielectric model at 1.4 GHz for a tundra organic-rich soil thawed and frozen. In: IEEE International Geoscience and Remote Sensing Symposium (IGARSS), Milan, Italy. 26–31 July 2015. IEEE, Piscataway, NJ. p. 2016–2019. doi:10.1109/IGARSS.2015.7326194

Mironov, V.L., L.G. Kosolapova, and S.V. Fomin. 2009. Physically and mineralogically based spectroscopic dielectric model for moist soils. IEEE Trans. Geosci Remote Sens. 47:2059–2070. doi:10.1109/TGRS.2008.2011631

Mironov, V.L., K.V. Muzalevskiy, and I.V. Savin. 2013. Retrieving temperature gradient in frozen active layer of arctic tundra soils from radiothermal observations in L-band: Theoretical modeling. IEEE J. Sel. Top. Appl. Earth Obs. Remote Sens. 6:1781–1785. doi:10.1109/JSTARS.2013.2262108

Miyamoto, T., T. Annaka, and J. Chikushi. 2003. Soil aggregate structure effects on dielectric permittivity of an Andisol measured by time domain reflectometry. Vadose Zone J. 2:90–97. doi:10.2136/vzj2003.9000

National Water and Climate Center. 2018a. Soil Climate Analysis Network (SCAN) data & products. Natl. Water Clim. Ctr., Portland, OR. https://www.wcc.nrcs.usda.gov/scan/

National Water and Climate Center. 2018b. Snow telemetry (SNOTEL) and snow course data and products. Natl. Water Clim. Ctr., Portland, OR. https://www.wcc.nrcs.usda.gov/snow/

O'Neill, P., and T. Jackson. 1990. Observed effects of soil organic matter content on the microwave emissivity of soils. Remote Sens. Environ. 31:175–182. doi:10.1016/0034-4257(90)90087-3

O'Neill, P., S. Chan, E. Njoku, T. Jackson, and R. Bindlish. 2015. Algorithm theoretical basis document (ATBD): Level 2 & 3 Soil Moisture (Passive) Data Products. Rev. B. Jet Propulsion Lab., California Inst. Technol., Pasadena.

Park, C.-H., A. Behrendt, E. LeDrew, and V. Wulfmeyer. 2017. New approach for calculating the effective dielectric constant of the moist soil for microwaves. Remote Sens. 9:732. doi:10.3390/rs9070732

Rautiainen, K., J. Lemmetyinen, J. Pulliainen, J. Vehvilainen, M. Drusch, A. Kontu, et al. 2012. L-band radiometer observations of soil processes in boreal and subarctic environments. IEEE Trans. Geosci. Remote Sens. 50:1483–1497. doi:10.1109/TGRS.2011.2167755

Rawls, W.J., D. Brakensiek, and K. Saxtonn. 1982. Estimation of soil water properties. Trans. ASAE 25:1316–1320. doi:10.13031/2013.33720

Reichle, R.H., J.V. Ardizzone, G.-K. Kim, R.A. Lucchesi, E.B. Smith, and B.H. Weiss. 2015. Soil Moisture Active Passive (SMAP) mission Level 4 surface and root zone soil moisture (L4_SM) product specification document. Jet Propulsion Lab., California Inst. Technol., Pasadena.

Reichle, R.H., G.J. De Lannoy, Q. Liu, J.V. Ardizzone, F. Chen, A. Colliander, et al. 2016. Soil Moisture Active Passive Mission L4_SM data product assessment (version 2 validated release). GMAO Office Note 12. Goddard Space Flight Ctr., Greenbelt, MD. https://ntrs.nasa.gov/archive/nasa/casi.ntrs.nasa.gov/20160008109.pdf

Reichle, R.H., G.J. De Lannoy, Q. Liu, R.D. Koster, J.S. Kimball, W.T. Crow, et al. 2017. Global assessment of the SMAP Level-4 surface and root-zone soil moisture product using assimilation diagnostics. J. Hydrometeorol. 18:3217–3237. doi:10.1175/JHM-D-17-0130.1

Robinson, D., S.B. Jones, J. Blonquist, and S. Friedman. 2005. A physically derived water content/permittivity calibration model for coarse-textured, layered soils. Soil Sci. Soc. Am. J. 69:1372–1378. doi:10.2136/sssaj2004.0366

Robinson, D., S.B. Jones, J. Wraith, D. Or, and S. Friedman. 2003. A review of advances in dielectric and electrical conductivity measurement in soils using time domain reflectometry. Vadose Zone J. 2:444–475. doi:10.2136/vzj2003.4440

Roth, C., M. Malicki, and R. Plagge. 1992. Empirical evaluation of the relationship between soil dielectric constant and volumetric water content as the basis for calibrating soil moisture measurements by TDR. J. Soil Sci. 43:1–13. doi:10.1111/j.1365-2389.1992.tb00115.x

Saxton, K., and W. Rawls. 2006. Soil water characteristic estimates by texture and organic matter for hydrologic solutions. Soil Sci. Soc. Am. J. 70:1569–1578. doi:10.2136/sssaj2005.0117

Schaap, M., D. Robinson, S.P. Friedman, and A. Lazar. 2003. Measurement and modeling of the dielectric permittivity of layered granular media using time domain reflectometry. Soil Sci. Soc. Am. J. 67:1113–1121. doi:10.2136/sssaj2003.1113

Seyfried, M., L. Grant, E. Du, and K. Humes. 2005. Dielectric loss and calibration of the Hydra Probe soil water sensor. Vadose Zone J. 4:1070–1079. doi:10.2136/vzj2004.0148

Stenberg, B., R.A.V. Rossel, A.M. Mouazen, and J. Wetterlind. 2010. Visible and near infrared spectroscopy in soil science. Adv. Agron. 107:163–215.

Stoffregen, H., T. Zenker, and G. Wessolek. 2002. Accuracy of soil water content measurements using ground penetrating radar: Comparison of ground penetrating radar and lysimeter data. J. Hydrol. 267:201–206. doi:10.1016/S0022-1694(02)00150-6

Topp, G., J. Davis, and A.P. Annan. 1980. Electromagnetic determination of soil water content: Measurements in coaxial transmission lines. Water Resour. Res. 16:574–582. doi:10.1029/WR016i003p00574

Tóth, B., M. Weynants, A. Nemes, A. Makó, G. Bilas, and G. Tóth. 2015. New generation of hydraulic pedotransfer functions for Europe. Eur. J. Soil Sci. 66:226–238. doi:10.1111/ejss.12192

Van de Griend, A.A., and J.-P. Wigneron. 2004. The *b*-factor as a function of frequency and canopy type at H-polarization. IEEE Trans. Geosci Remote Sens. 42:786–794. doi:10.1109/TGRS.2003.821889

Vereecken, H., J. Maes, J. Feyen, and P. Darius. 1989. Estimating the soil moisture retention characteristic from texture, bulk density, and carbon content. Soil Sci. 148:389–403. doi:10.1097/00010694-198912000-00001

Wagner, N., T. Bore, J.C. Robinet, D. Coelho, F. Taillade, and S. Delepine-Lesoille. 2013. Dielectric relaxation behavior of Callovo–Oxfordian clay rock: A hydraulic-mechanical-electromagnetic coupling approach. J. Geophys. Res. Solid Earth 118:4729–4744. doi:10.1002/jgrb.50343

Wang, J., and B. Choudhury. 1981. Remote sensing of soil moisture content, over bare field at 1.4 GHz frequency. J. Geophys. Res. Oceans 86:5277–5282. doi:10.1029/JC086iC06p05277

Wang, J.R. 1983. Passive microwave sensing of soil moisture content: The effects of soil bulk density and surface roughness. Remote Sens. Environ. 13:329–344. doi:10.1016/0034-4257(83)90034-2

Wang, J.R., and T.J. Schmugge. 1980. An empirical model for the complex dielectric permittivity of soils as a function of water content. IEEE Trans. Geosci. Remote Sens. GE-18:288–295. doi:10.1109/TGRS.1980.350304

Watanabe, M., G. Kadosaki, Y. Kim, M. Ishikawa, K. Kushida, Y. Sawada, et al. 2012. Analysis of the sources of variation in L-band backscatter from terrains with permafrost. IEEE Trans. Geosci Remote Sens. 50:44–54. doi:10.1109/TGRS.2011.2159843

Wigneron, J.-P., T. Jackson, P. O'Neill, G. De Lannoy, P. De Rosnay, J. Walker, et al. 2017. Modelling the passive microwave signature from land surfaces: A review of recent results and application to the L-band SMOS & SMAP soil moisture retrieval algorithms. Remote Sens. Environ. 192:238–262. doi:10.1016/j.rse.2017.01.024

Wigneron, J.-P., L. Laguerre, and Y.H. Kerr. 2001. A simple parameterization of the L-band microwave emission from rough agricultural soils. IEEE Trans. Geosci Remote Sens. 39:1697–1707. doi:10.1109/36.942548

Wösten, J., A. Lilly, A. Nemes, and C. Le Bas. 1999. Development and use of a database of hydraulic properties of European soils. Geoderma 90:169–185. doi:10.1016/S0016-7061(98)00132-3

Yang, F., G.-L. Zhang, J.-L. Yang, D.-C. Li, Y.-G. Zhao, F. Liu, et al. 2014. Organic matter controls of soil water retention in an alpine grassland and its significance for hydrological processes. J. Hydrol. 519:3086–3093. doi:10.1016/j.jhydrol.2014.10.054

Yi, Y., J.S. Kimball, R.H. Chen, M. Moghaddam, and C.E. Miller. 2019. Sensitivity of active layer freezing process to snow cover in arctic Alaska. Cryosphere 13:197–218. doi:10.5194/tc-13-197-2019